

A Hyper-weight Network for Hyperspectral Image Denoising

Xiangyu Rui, Xiangyong Cao, Jun Shu, Qian Zhao and Deyu Meng

Abstract—In the hyperspectral image (HSI) denoising task, the real noise embedded in the HSI is always complex and diverse so that many model-based HSI denoising methods only perform well on some specific noisy HSIs. To enhance the noise adaptation capability of current methods, we first resort to the weighted HSI denoising model since its weight is capable of characterizing the noise in different positions of the image. However, the weight in these weighted models is always determined by an empirical updating formula, which does not fully utilize the noise information contained in noisy images and thus limits their performance improvement. In this work, we propose an automatic weighting scheme to alleviate this issue. Specifically, the weight in the weighted model is predicted by a hyper-weight network (i.e., HWnet), which can be learned in a bi-level optimization framework based on the data-driven methodology. The learned HWnet can be explicitly plugged into other weighted denoising models, and help adjust weights for different noisy HSIs and different weighted models. Extensive experiments verify that the proposed HWnet can help improve the generalization ability of a weighted model to adapt to more complex noise, and can also strengthen the weighted model by transferring the knowledge from another weighted model. Additionally, to explain the experimental results, we also theoretically prove the training error and generalization error upper bound of the proposed HWnet, which should be the first generalization error analysis in the low-level vision field as far as we know.

Index Terms—Hyperspectral image denoising, weighted model, bi-level optimization, learning theory.

arXiv:2301.06081v1 [eess.IV] 9 Dec 2022

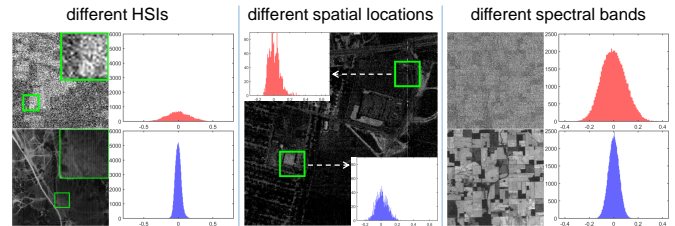
1 INTRODUCTION

HYPERSPECTRAL images (HSIs), captured by measuring the electromagnetic spectrum of a scene across many bands, provide richer information than typical RGB images and can be widely used in many fields, such as remote sensing [1], agriculture [2], food industry [3], and biology [4]. However, the collected HSIs by hyperspectral sensors are often degraded by diverse noise sources including shot noise, dark current noise and thermal noise [5]. The undesired degradation would inevitably affect subsequent HSI applications, and thus HSI denoising is an important pre-processing step to improve the image quality for further downstream tasks.

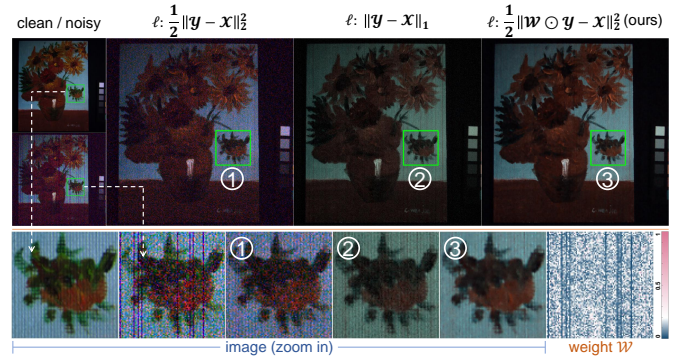
HSI denoising aims to restore the clean image $\mathcal{X} \in \mathbb{R}^{h \times w \times b}$ from the observed noisy image $\mathcal{Y} \in \mathbb{R}^{h \times w \times b}$. Mathematically, the HSI denoising task can be formulated as the following optimization problem:

$$\hat{\mathcal{X}} = \arg \min_{\mathcal{X}} \ell(\mathcal{Y}, \mathcal{X}) + \lambda R(\mathcal{X}), \quad (1)$$

where $\hat{\mathcal{X}} \in \mathbb{R}^{h \times w \times b}$ is the restored image, $\ell(\cdot, \cdot)$ is the loss term that measures the discrepancy between the noisy image \mathcal{Y} and the clean image \mathcal{X} , $R(\cdot)$ is the regularization term that imposes explicit prior on the clean image to make the problem well-posed, and λ is the trade-off param-



(a) Histogram of estimated noise.



(b) Effectiveness of loss term choice. The weight \mathcal{W} is predicted by HWnet and can essentially deliver complex noise structure.

Figure 1: (a) Examples of real noisy HSIs, along with the histograms of their contained noise roughly estimated by SVD; (b) A noisy image with deadline noise, as well as its underlying clean one, and denoising results obtained under ℓ_2 (NNM), ℓ_1 (RPCA) and the weighted ℓ_2 (ours) loss term settings. The lower-right shows the weight mapping obtained by our HW-Net from the noisy image.

- Xiangyu Rui, Jun Shu, Qian Zhao and Deyu Meng are with School of Mathematics and Statistics and Ministry of Education Key Lab of Intelligent Networks and Network Security, Xi'an Jiaotong University, Xi'an 710049, China.
E-mail: xyryui.aca, xjtushujun@gmail.com, timmy.zhaoqian, dymeng@mail.xjtu.edu.cn
- Xiangyong Cao is with School of Computer Science and Technology and Ministry of Education Key Lab For Intelligent Networks and Network Security, Xi'an Jiaotong University, Xi'an 710049, China.
E-mail: caoxiangyong@xjtu.edu.cn

ter to balance the loss and regularization terms. From a maximum likelihood estimation (MLE) perspective, we can easily deduce that the form of loss function corresponds to

the distribution of additive noise. For example, the ℓ_2 and ℓ_1 loss terms correspond to the cases where the additive noise follows i.i.d. Gaussian and Laplacian distributions, respectively [6]. But in real cases, the HSI noise might be much more complex than such pre-assumed simple noise forms. Fig. (1b) shows a typical HSI instance, containing additive deadline noise, which is difficult to use a simple distribution to describe, and thus the ℓ_1 and ℓ_2 loss terms don't perform well in this case. Therefore, to guarantee a good HSI denoising effect, we need to carefully design the loss function to make it properly comply with the complex and diverse HSI noises, as clearly shown in Fig. (1a).

To alleviate this issue, existing HSI denoising methods are often proposed from the following two aspects. The first is to subjectively assume the noise distribution as a broad class of distributions in advance as aforementioned [6]–[9] since the real noise distribution is unknown. This type of methods often corresponds to one weighted loss optimization problem as a necessary sub-step of the optimization process. The second is to directly utilize the weighted loss to capture this noise property [10], to make the method more flexibly fit different noise patterns in spatial and spectral dimensions of HSI. To sum up, the weighted loss is a popular choice for the HSI denoising problem. The weighted HSI denoising model can be generally expressed as:

$$\hat{\mathcal{X}} = \arg \min_{\mathcal{X}} \|\mathcal{W} \odot (\mathcal{Y} - \mathcal{X})\| + \lambda R(\mathcal{X}), \quad (2)$$

where $\mathcal{W} \in \mathbb{R}^{h \times w \times b}$ is the weight tensor, which aims to capture the noise intensity of each position in the image. However, this model usually requires pre-setting the weight tensor before conducting the denoising process, and the aforementioned two types of weighted loss approaches implement this goal either by assigning the unknown distribution subjectively or fixing the weight tensor empirically, making them hardly be adaptively and properly used in complex scenarios.

To tackle this critical issue, in this paper, we focus on designing a novel method to adaptively learn the weight for the weighted HSI denoising model. Specifically, we propose an automatic weighting scheme to predict the weight tensor. Instead of being preset or updated manually, in our method the weight tensor is set automatically by a neural network h_θ (called hyper-weight network or HWnet), which takes the noisy HSI as input and generates the weight as the output. We then design a data-driven approach to learn the HWnet. Once the HWnet is learned, it can be readily used to estimate the weight for other pre-unseen noisy HSIs. In particular, we can train the HWnet using a collection of clean/noisy HSI training pairs contaminated by one or more noise types and then apply the trained HWnet to predict the weight of a new noisy HSI. Therefore, the proposed weighting strategy can be used in an essential plug-and-play (PnP) manner and hopefully enable a weighted HSI denoising model to adaptively match the noise patterns for different HSIs. In other words, this weighting methodology can transfer the noise knowledge learned from some given noise types to other unseen noise types, and thus help enhance the generalization ability of the weighted HSI denoising model to adapt to more complex noise.

As aforementioned, the HWnet should first be trained

before being applied to new HSIs, and the training is implemented by coupling with several specific traditional weighted HSI denoising models, called the source models. Since the goal of learning the HWnet is to better denoise the noisy HSI by solving the source models, determining the HWnet can then be naturally formulated as a bi-level optimization problem, which is composed of two sub-problems. The lower level sub-problem aims to generate the restored HSI by optimizing each source model with the weight fixed, and thus the restored HSI depends on the parameters of the HWnet. For the upper level sub-problem, it is proposed based on the data-driven idea, and aims to learn the parameters of the HWnet by minimizing the discrepancy between the restored and corresponding ground-truth HSIs given the noisy/clean training pairs. To solve the proposed bi-level optimization problem, the lower level problem is first iteratively optimized, and then the upper level problem is optimized. When the whole optimization process is finished, the denoised HSIs and the parameters of the HWnet can be obtained simultaneously. Then, the learned HWnet can be regarded as a weight predictor for general noisy HSIs. It should be noted that the recovered HSI from the lower level problem is also related to the regularization term, and thus the trained HWnet is capable of acquiring prior knowledge of the regularization term besides the noise knowledge. In the circumstances, it is natural to query whether the trained HWnet from one or more denoising models can be transferred to other weighted denoising models with different regularization terms in a PnP manner. In other words, we aim to exploit the generalization ability of our HWnet across different HSI denoising models.

Based on the proposed bi-level learning framework for the automatic weighting scheme, we then focus on studying the generalization ability of the HWnet across different HSI datasets and different HSI denoising models. Firstly, to analyze the generalization ability of our HWnet across different datasets, we conduct comprehensive experiments. The experimental results substantiate that the HWnet trained on one type of noise is capable of promoting the denoising performance of the weighted model on other unseen noisy HSIs. Secondly, to analyze the generalization error of the HWnet across different models, we take the integration of theoretical analysis and experimental evaluation. Specifically, when the trained HWnet is applied to new HSI denoising models whose regularization terms are different from those of the source models, we prove a theoretical upper bound for the generalization error under the general framework of learning theory from the view of task diversity. Besides, to accomplish the proposed theory, we also present the training error of our HWnet.

In summary, the contribution of this study is as follows:

- 1) We propose an automatic weighting scheme to predict the weight of a weighted HSI denoising model through a hyper-weight network (i.e., HWnet) learned by a bi-level optimization framework. Different from most current methods requiring manually pre-assuming noise/loss form or pre-setting explicit weight function, the proposed HWnet is implemented in a purely data-driven manner and

- can adaptively fit noise patterns underlying data.
- 2) The learned HWnet can automatically adjust weights for different noisy HSIs. Besides, it can also be explicitly plugged into general weighted HSI denoising models to promote their complex noise adaptability. Extensive experiments have verified the generalization ability of HWnet across different HSI noise patterns and diverse HSI denoising models. Besides, experimental results confirm that the predicted weight by HWnet can be explicitly plugged into other kinds of HSI denoising models (e.g., deep image prior model) to improve their denoising performance.
 - 3) We theoretically prove the generalization error upper bound of our proposed HWnet to verify its generalization capability across different denoising models. As far as we know, this should be the first work to theoretically analyze the generalization error bound across different models in the low-level vision field.

The rest of this work is organized as follows. Sec. 2 reviews existing HSI denoising models and presents some relevant learning theory works. Sec. 3 presents our proposed automatic weighting scheme. Sec. 4 demonstrates experiments to verify the generalization ability of our HWnet both on different noise patterns and different models. Additionally, the theoretical analysis of training and generalization errors of our method is provided in Sec. 5 to support the experimental results. The paper is then concluded.

2 RELATED WORKS

In this section, we will briefly review the existing HSI denoising methods and some related learning theory research.

2.1 HSI Denoising Methods

Existing HSI denoising methods can be roughly divided into two categories, i.e. model-based approaches and deep-learning-based ones. In the following, we will introduce the two types of methods separately.

2.1.1 Model-based HSI Denoising Approaches

The model-based HSI denoising methods aim to restore the clean HSI by fully investigating the image priors. One of the most important HSI prior is the low-rank property, mainly characterizing the evident correlation along the spectral dimension of general HSIs. One typical method is LRMR [11], which formulates HSI denoising as a robust nuclear norm minimization (NNM) model. Subsequently, [12] proposed to spatially split the HSI into patches and then solve the NNM problem with noise level adjustment. Beyond the convex nuclear norm regularizer, [13] further proposed a non-convex regularizer to induce sparsity. Regarding the HSI as a three-dimensional tensor, low-rank tensor decomposition approaches have also attracted much attention. Typically, [14] used CANDECOMP/PARAFAC decomposition and the average nuclear norm along each mode to describe the low-rank property. [15] considered Tucker decomposition and the sparsity on the core tensor. [16] applied tensor-ring decomposition to better preserve the HSI intrinsic property. [17] used t-SVD to describe tensor low-tubal rankness.

Another widely used HSI prior is the total variation (TV), which encodes the smoothness prior of HSIs along both spectral and spatial dimensions [18]–[23]. For example, [18] used the weighted Frobenius norm on the gradient map as regularization. [19] applied spectral difference operator on spatial gradient map to additionally describe the HSI spectral correlation. [20] proposed an enhanced TV regularization by calculating sparsity on subspace bases of gradient maps along all bands of an HSI. Sparse representation is also a commonly used prior to capture the sparsity of representative coefficients under some bases. Typically, [24] considered measuring the spatial and spectral correlation of an HSI and then used the correlation to split the HSI into patches before performing sparse representation. [25] applied modified structured sparse coding to capture the underlying HSI prior. Additionally, more recent researches consider several HSI priors simultaneously. Along this line, [21] jointly utilized the low-rank property in the spectral dimension and the total variation constraint in the spatial dimension. [26] applied both sparse representation and low-rank constraint to formulate the denoising model. Other prior properties of HSI have also been attempted. E.g., [27] took mode-2 unfolding of an HSI with more low rankness than the other two modes. [28] performed low rank matrix decomposition along the spectral mode and used WNNM [29] to denoise the reduced image. [10] placed group sparsity on the gradient maps of the reduced image and also set the continuity constraint on the spectral factor matrix.

In addition to exploiting HSI priors, designing a proper loss term to describe the noise property is also an alternative. Typical methods assume HSI mainly contains two types of noise, i.e., Gaussian noise and sparse noise, and adopt ℓ_2 and ℓ_1 losses to tackle the noise separately. Specifically, [12] pre-estimated the noise variance of each band and then proposes a vague weighted ℓ_2 model whose weights are directly related to noise variance by a fixed empirical mapping. [30] utilized a $\ell_{2,1}$ -norm loss to robustly handle noise and outliers. [10] applied the weighted ℓ_1 loss term where the weight is proportional to the sparse residual for each iteration [31]. Another series of methods is called noise modeling [6]–[9], which firstly assumes the HSI noise follows a broad class of distribution and then constructs the loss function based on the maximum likelihood estimation (MLE) or variational inference (VI) principle. For example, [6] assumed the additive noise obeys the mixture of Gaussian (MoG) distribution which theoretically can approximate any continuous distribution. Later, [7] established a mixture of exponential power (MoEP) distribution to model the noise. Further, [8] claimed that the noise in a natural HSI is always with a more complicated non-independent and identically distributed (non-i.i.d) structure. [9] hypothesized that the noise of HSI in each band is depicted by a Dirichlet process Gaussian mixture model (DP-GMM). Similarly, [32] applied the mixture of Gaussian (MoG) distribution to model noise and the corresponding M-step corresponds to a weighted ℓ_2 model. [33] classified the noise patterns using MoG and only used the Gaussian-noise-whitened components to restore the HSI. In summary, most of the above HSI denoising models are essentially weighted-loss models, where the weight is specified subjectively or empirically. In this work, instead of pre-defining the weight update

equation empirically or pre-assuming the noise distribution subjectively, we design a novel approach to make this weight setting aim able to be automatically implemented¹.

2.1.2 Deep-Learning-based HSI Denoising Approaches

Recently, deep learning (DL) methods have been extensively studied in the HSI denoising problem, where denoising is implemented by learning an explicit nonlinear mapping from noisy/clean HSI pairs. [35] is the first work to adopt a convolutional neural network (CNN) for HSI denoising, where 2D convolution and dilation convolution are used. Later, [36] fused the adjacent bands of HSI to utilize both the spatial and spectral features in the deep residual CNN. [37] further applied 3D convolution instead of 2D convolution together with self-attention to extract HSI features. [38] also adopted 3D convolution, quasi-recurrent pooling function, and alternating directional structure to design the network. Besides, [39] combined the matrix factorization method with CNN, where the CNN is used as a solver of the corresponding sub-problem. [40] used two reasoning modules to carefully extract both global and local spatial-spectral features. [41] designed a new HSI denoising network by combining the CNN and transformer. Further, to tackle the physical interpretability issue of the deep neural network (DNN), [42], [43] proposed a model-guided spectral-spatial network by unfolding the iterative algorithm to solve the sparse model. Afterwards, [44] introduced an end-to-end model-aided non-local neural network to simultaneously consider the spectral low-rank model and spatial deep prior. Although the aforementioned DL-based HSI denoising methods have achieved excellent performance in many applications, their performance largely relies on complex network architecture design and the quality and quantity of training data, and often lacks good generalization capability.

2.2 Learning Theory on Generalization

The learning theory serves as the cornerstone for the machine learning fields and has been closely concerned for decades. It has gained great development in transfer learning [45] [46], domain adaption [47] [48] [49] [50], domain generalization [51] [52] [53] [54], and so on. For example, [55] [56] considered the generalization theory of the method that learns the common representation from several training tasks and generalizes to new tasks from the perspective of task diversity. [57] studied the generalization theory of the approach that learns a universal hyper-parameter prediction policy for a group of tasks. The generalization theories of these works are developed mainly based on a pre-assumed common environment that all tasks are drawn from. Additionally, the diversity of the environment should be bounded by the diversity of training tasks so that the generalization makes sense.

¹In our previous conference paper [34], we have made an early but relatively rough attempt on this issue. In this study, we have substantially extended the study from comprehensive perspectives throughout model, algorithm, theory and experiment. Specifically, the essential extension includes rebuilding the learning framework, more comprehensive theoretical evidence, more sufficient experiments and more intrinsic analysis of the working scheme underlying the learned weighting scheme. Please see more details in our supplemental file.

Table 1: Necessary notations in our proposed method

$\ X\ _*$	the sum of singular values of X
$a * b$	the multiplication between a and b
$a \times b$	the size of a matrix
A/B	element-wise division
A^2	element-wise square
$A \geq (\leq) B$	element-wise comparison
\odot	element-wise multiplication
$\ \cdot\ _2$	Frobenius norm for matrices and tensors, or l_2 norm for vectors
$\langle \cdot, \cdot \rangle$	inner product
$\mathcal{N}(0, 1)$	standard Gaussian distribution
\mathbb{E}	expectation
$[N]$	$\{1, 2, \dots, N\}$

In this study, inspired by these related generalization researches, we prove the generalization theory of our proposed weight prediction scheme for the HSI denoising model. The main differences between our method and other generalization theories are as follows. Firstly, we turn to measuring the individual task divergence rather than the abstract environment, which is more pertinent to our problem. Secondly, the existing generalization theory works mainly focus on high-level classification problems, while our work should be the first generalization theory work in the low-level vision field to the best of our knowledge.

3 PROPOSED MODEL

In this section, we first introduce our proposed automatic weighting scheme for the weighted HSI denoising model. Then, we design a data-driven bi-level optimization framework to learn the weight prediction network. We depict necessary notations in Table 1 for notation convenience.

3.1 Automatic Weighting Scheme

As mentioned in the introduction section, the general weighted HSI denoising model is expressed in Eq. (2). Here we adopt the general ℓ_2 loss in our HSI denoising model, which is expressed as:

$$\min_{\mathcal{X}} \frac{1}{2} \|\mathcal{W} \odot (\mathcal{Y} - \mathcal{X})\|_2^2 + \lambda R(\mathcal{X}), \quad (3)$$

where \mathcal{W} is the weight tensor that helps to adapt to diverse noise distribution in each pixel (i.e., spectral vector) of the HSI. Traditional methods for solving Eq. (3) are generally composed of two steps. Firstly, \mathcal{W} is adjusted according to some empirical weight or noise distribution presetting methods, and then problem (3) is solved by certain optimization techniques. In this paper, we propose an automatic weight prediction method to alleviate the manual weight setting issue in the first step. Specifically, we design a neural network, called hyper-weight network or HWnet, to estimate the weight tensor \mathcal{W} , namely

$$\mathcal{W} = h_{\theta}(\mathcal{Y}), \quad (4)$$

where $h_{\theta}(\cdot)$ is a hyper-weight network (i.e., HWnet) with parameter θ , which receives the noisy HSI \mathcal{Y} as the input and generates the weight \mathcal{W} as the output. Then, our

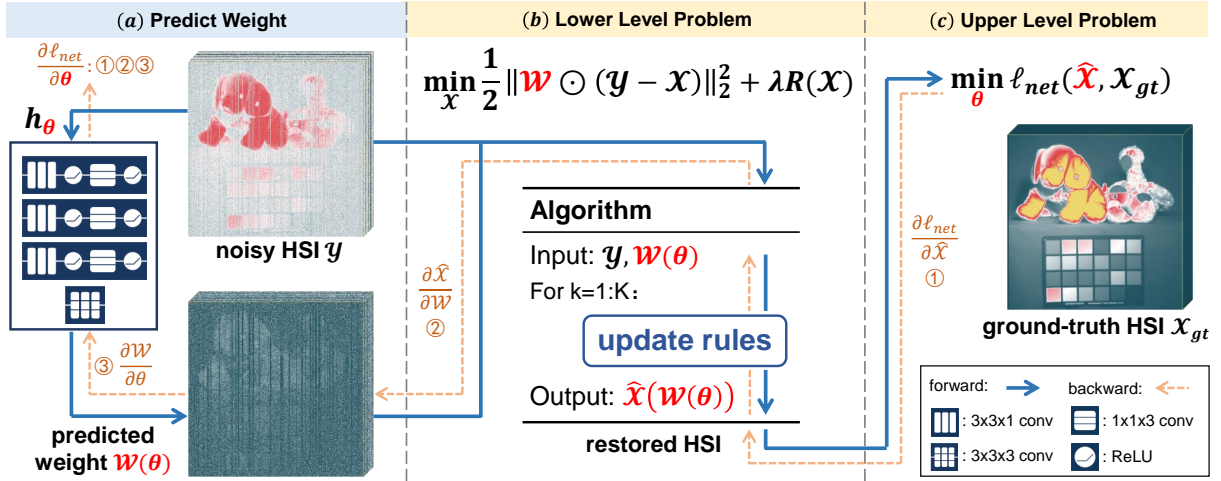


Figure 2: The overall bi-level training strategy for the proposed weighting scheme. (a) is the first step to predict weight \mathcal{W} for an observed noisy HSI \mathcal{Y} using HWnet h_θ . (b)-(c) are bi-level optimization steps. In (b), the noisy HSI \mathcal{Y} and the predicted weight \mathcal{W} are sent to weighted denoising models (here only one training task is present in the figure), and the weighted problems produce restored HSI $\hat{\mathcal{X}}$. In (c), h_θ is learned by minimizing the training loss ℓ_{net} . According to the chain rule, the gradients of θ is calculated by $\partial \ell_{net} / \partial \hat{\mathcal{X}}$, $\partial \hat{\mathcal{X}} / \partial \mathcal{W}$ and $\partial \mathcal{W} / \partial \theta$.

automatic weighting scheme for the HSI denoising model is built by combining Eq. (3) and Eq. (4). Once the HWnet is trained (i.e., the parameter θ is learned), it can be readily used for setting the weight for general noisy HSI \mathcal{Y} . The denoised HSI \mathcal{X} can then be directly obtained by solving Eq. (3) without the need to further pre-set the weights or assume the underlying noise distributions.

In this work, the HWnet h_θ is designed as a simple four-layer convolutional neural network (CNN). Similar to [34], the first three layers of h_θ borrow the “pseudo 3D” convolution structure [58], which takes the form of “ $3 \times 3 \times 1$ conv + ReLU + $1 \times 1 \times 3$ conv”. Each layer is followed by “ReLU” activation function. Batch normalization is not used since it inclines to decrease the noise distinction between data. The final layer takes the full “ $3 \times 3 \times 3$ ” convolution. The output of the final convolutional layer is activated by the softmax function and then multiplies $h * w * b$. Thus the predicted \mathcal{W} is averaged to 1.

Next, we will introduce the proposed bi-level optimization framework for learning the parameter θ of the HWnet.

3.2 HWnet Training

The minimum point of the optimization problem (3) is the restored HSI \mathcal{X} , which has an implicit relationship with the weight \mathcal{W} since different \mathcal{W} s would result in different \mathcal{X} s. Further, \mathcal{X} can be considered as a function of \mathcal{Y} and θ since \mathcal{W} is parameterized by θ (i.e. $\mathcal{W} = h_\theta(\mathcal{Y})$). Therefore, the minimum point of (3) can be written as

$$\hat{\mathcal{X}}(\mathcal{Y}, \theta) := \arg \min_{\mathcal{X}} \frac{1}{2} \|h_\theta(\mathcal{Y}) \odot (\mathcal{Y} - \mathcal{X})\|_2^2 + \lambda R(\mathcal{X}). \quad (5)$$

Next, we will first show how to train HWnet in the bi-level framework with single source model in detail. Then, it can be naturally extended into multiple source models case.

3.2.1 HWnet Training with Single Source Model

As emphasized in the introduction section, the weight \mathcal{W} is expected to help the weighted HSI denoising model to

better remove the noise from the noisy HSI \mathcal{Y} . Inspired by the data-driven methodology, a natural idea of learning the parameter θ of HWnet is to minimize the distance between the restored HSI $\hat{\mathcal{X}}(\mathcal{Y}, \theta)$ calculated from the low level optimization problem and the ground-truth HSI \mathcal{X}_{gt} pre-given under the paired training data $\{(\mathcal{Y}_i, \mathcal{X}_{gt_i})\}_{i=1}^N$. This idea can be mathematically formulated as a bi-level optimization problem as follows:

$$\min_{\theta} \frac{1}{N} \sum_{i=1}^N \ell_{net}(\hat{\mathcal{X}}_i(\theta), \mathcal{X}_{gt_i}), \quad (6a)$$

$$\hat{\mathcal{X}}_i(\theta) = \arg \min_{\mathcal{X}} \frac{1}{2} \|\mathcal{W}_i \odot (\mathcal{Y}_i - \mathcal{X})\|_2^2 + \lambda R(\mathcal{X}), \quad (6b)$$

where ℓ_{net} is the training loss for each pair, $\mathcal{W}_i = h_\theta(\mathcal{Y}_i)$, $i \in [N]$, and N is the number of training pairs. Each noisy HSI \mathcal{Y}_i corresponds to its own weight \mathcal{W}_i . The lower level problem (6b) is the weighted HSI denoising model, and the upper level problem (6a) is about minimizing the training loss between the restored images obtained from the lower-level problem and their groundtruths.

To solve this bi-level optimization problem, we utilize a simple yet efficient way. Firstly, we write down the solving scheme $\hat{\mathcal{X}}_i(\theta)$ of the lower level optimization problem (6b) in an explicit manner, and then send this explicit scheme to the upper problem (6a). Specifically, the lower level problem can be solved by employing some commonly used algorithms, such as proximal gradient (PG) [59], half quadratic splitting (HQS) [60] and alternating direction method of multipliers (ADMM) [61]. Suppose that the derivative $\partial \hat{\mathcal{X}}_i / \partial \mathcal{W}_i$ exists and is tractable, and then the upper level problem can be solved by some popular optimizers, e.g., stochastic gradient descent (SGD). By using the chain rule, the network parameter θ can be updated by:

$$\theta \leftarrow \theta - \alpha \frac{1}{N} \sum_{i=1}^N \frac{\partial \ell_{net}}{\partial \hat{\mathcal{X}}_i} \frac{\partial \hat{\mathcal{X}}_i}{\partial \mathcal{W}_i} \frac{\partial \mathcal{W}_i}{\partial \theta}, \quad (7)$$

where α is the learning rate.

Let's take the weighted nuclear norm minimization (WNNM) model as an example, where the regularization R is the nuclear norm $\|\cdot\|_*$. This WNNM model acts as the lower level optimization problem of (6b), and the corresponding bi-level optimization problem is defined as:

$$\min_{\theta} \frac{1}{N} \sum_{i=1}^N \ell_{net}(\hat{\mathcal{X}}_i(\theta), \mathcal{X}_{gt_i}), \quad (8a)$$

$$\hat{\mathcal{X}}_i(\theta) = \arg \min_{\mathcal{X}} \frac{1}{2} \|h_{\theta}(\mathcal{Y}_i) \odot (\mathcal{Y}_i - \mathcal{X})\|_2^2 + \lambda \|\mathcal{X}\|_*. \quad (8b)$$

To solve the above bi-level optimization problem, we firstly apply the augmented Lagrange multiplier (ALM) [62] to solve the lower level problem. The detailed derivation of the algorithm is presented in the supplemental materials, and the whole iterative process is summarized in Algorithm 1. The operators involved in Algorithm 1 are singular value decomposition (SVD), shrinkage operator, and basic operations between matrices. The algorithm can then be seen as an explicit mapping from the input image Y to the restored image $\hat{X}(\theta)$, and gradients or subgradients are computable for all its involved operators, and thus $\partial \hat{X} / \partial W$ is tractable. In this work, we implement Algorithm 1 with a K -stage network by unfolding its K iterative steps, whose computational graph is shown in Fig. 3. In the network, each stage corresponds to one iteration step of this algorithm. After implementing the ALM algorithm to the lower level problem, the parameter θ of HWnet can thus be learnable. The output of Algorithm 1 is an approximated solution $\hat{X}(\theta)$, which is then sent to ℓ_{net} in the upper level problem. Finally, we use gradient descent based algorithm to optimize the parameter θ and then obtain the trained HWnet h_{θ} .

Fig. 2 summarizes the whole training process of the bi-level problem (6a)-(6b). The "Algorithm" refers to Algorithm 1 when specifically solving (8a)-(8b), and can be replaced by other properly designed algorithms when solving other source models.

3.2.2 HWnet Training with Multiple Source Models

In Sec. 3.2.1, we discuss the training of HWnet h_{θ} from a single HSI denoising model (3) under the bi-level framework (6a)-(6b). This framework can be naturally extended to a more general bi-level learning framework where the parameter of HWnet is learned from multiple HSI denoising models, which is mathematically formulated as:

$$\min_{\theta} \frac{1}{T} \sum_{t=1}^T \frac{1}{N_t} \sum_{i=1}^{N_t} \ell_{net}(\hat{\mathcal{X}}_{ti}(\theta), \mathcal{X}_{gt_{ti}}), \quad (9a)$$

$$\hat{\mathcal{X}}_{ti}(\theta) = \arg \min_{\mathcal{X}} \frac{1}{2} \|\mathcal{W}_{ti} \odot (\mathcal{Y}_{ti} - \mathcal{X})\|_2^2 + \lambda_t R_t(\mathcal{X}), \quad (9b)$$

where $\mathcal{W}_{ti} = h_{\theta}(\mathcal{Y}_{ti})$, $i \in [N_t]$ and $t \in [T]$. The lower level problem (9b) contains T weighted denoising models with different regularizations $\{\lambda_t R_t\}_{t=1}^T$. The multiple-model framework can thus aggregate more model information to learn a unified HWnet. If T equals 1, the model degrades to the single model framework as presented in Sec. 3.2.1.

3.3 Applying HWnet to New Images/Models in PnP Way

Note that once the HWnet is learned from the single-model or multiple-model framework, it can be readily used to set

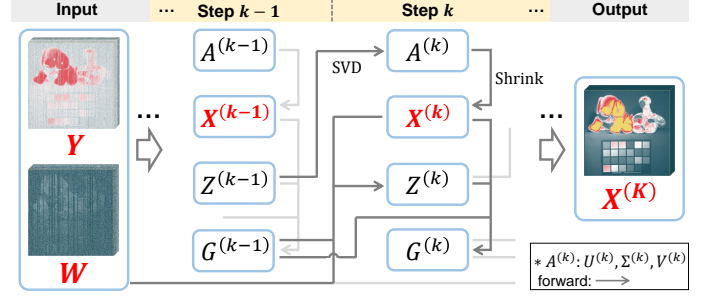


Figure 3: Computational graph of the forward process of solving the lower level optimization problem (i.e., WNNM model). Each node in the graph corresponds to one variable in each step. Here we omit μ and denote $A^{(k)} = \{U^{(k)}, \Sigma^{(k)}, V^{(k)}\}$ to simplify the diagram.

Algorithm 1 ALM algorithm to solve the WNNM model

Input: noisy image Y , weight $W = h_{\theta}(Y)$, iteration steps K , trade-off parameter λ .

Initialization: $Z^{(0)}, G^{(0)}, \mu^{(0)}, \rho$

- 1: **for** $k = 1 : K$ **do**
- 2: $U^{(k)} \Sigma^{(k)} V^{(k)T} = \text{SVD}(Z^{(k-1)})$,
- 3: $X^{(k)} = U^{(k)} \text{Shrink}(\Sigma^{(k)}, \frac{\lambda}{\mu^{(k-1)}}) V^{(k)T}$,
- 4: $Z^{(k)} = \frac{W^2 \odot Y + \mu^{(k-1)} X^{(k)} - G^{(k-1)}}{W^2 + \mu^{(k-1)}}$,
- 5: $G^{(k)} = G^{(k-1)} + \mu^{(k-1)} (X^{(k)} - Z^{(k)})$,
- 6: $\mu^{(k)} = \rho \mu^{(k-1)}$,
- 7: **end for**
- 8: **Output:** $X^{(K)}(\theta) \approx \hat{X}(\theta)$

weights for new images and new models in a PnP way. That is, in this stage, the upper level problem is not required to be considered, and we only need to directly employ this learned explicit weighting function into a new weighted HSI denoising model on a new noisy HSI. Specifically, on the one hand, since the HWnet is learned from the synthetic clean/noisy HSI pairs with diverse noises, it is expected to be able to capture the proper weight prediction rule for general noisy HSIs, and finely being used for HSIs with a wide range of complex noise types. On the other hand, since the trained HWnet is also expected to obtain the model regularization information besides the noise knowledge in the bi-level optimization framework, it is also rational to be transferably used to directly set weights on other target models with different regularization terms. In the next section, we will validate such image/model generalization capability of HWNet by experiments, and then provide some learning theory evidence from a theoretical perspective.

4 EXPERIMENTAL RESULTS

We then conduct experiments to verify the effectiveness of our proposed automatic weighting scheme for weighted HSI denoising models. For convenience, the weighted denoising models with HWnet are prefixed by "HW-".

Three basic weighted denoising models are used as source models to train HWnet, i.e., weighted model with nuclear norm (NNM) [11], weighted model with spatial total

Table 2: All combinations of source models

type \rightarrow	N	T	TS	N+T	N+TS	T+TS	N+T+TS
HW-NNM	✓			✓	✓		✓
HW-TV		✓		✓		✓	✓
HW-TVS			✓		✓	✓	✓

variation norm (TV) [63], and weighted model with spectral total variation norm (TVS) [63]. The NNM can enforce the bands of HSI to lie in a low dimensional subspace, and the total variation regularization characterizes the smoothness property in the spatial and spectral dimensions. As reviewed in the related work section, such low-rank and the spatial and spectral smoothness regularizers are the most commonly adopted ones in existing HSI denoising models. Thus these three weighted models are typical and can also bring convenience to analyzing the generalization behavior of HWnet as introduced in Sec. 4.2.1. The ALM algorithm is used to solve all of the three weighted denoising models due to its fast convergence and simple expression. Please see more algorithm details in the supplemental material.

In the general bi-level optimization framework (9a)-(9b), the above three denoising models can be generated as totally seven different combinations for the lower level problem (9b) to train the HWnet, as listed in Table 2. The abbreviations “N”, “T” and “TS” refer to the source tasks of HW-NNM, HW-TV and HW-TVS, respectively. Additionally, the “N+T” type means that we assemble the HW-NNM model and HW-TV model together to train the HWnet and the number of tasks T is two. Consequently, we train seven HWnets under the seven different model combinations.

To generate the training pairs, the CAVE dataset² is used, which contains 32 images of real-world materials and objects. Specifically, we randomly select 20 images to generate the training pairs. The original size of each image is $512 \times 512 \times 31$, and we crop 2500 overlapping patches with a size of $64 \times 64 \times 31$. After rotating and flipping, the total number of training patch pairs is augmented to 20000. Additionally, six HSI datasets are used for testing, including the remaining 10 images in the CAVE dataset, 10 images with a size of $512 \times 512 \times 31$ from ICVL dataset³, Washington DC Mall data⁴ with a size of $200 \times 200 \times 152$, PaviaU data⁵ with a size of $340 \times 340 \times 70$, Urban data⁶ and Indian Pines data. The first 4 testing datasets are used for synthetic HSI denoising experiments, and the last two datasets are used for real HSI denoising.

Firstly, we generate five kinds of complex noise for synthetic experiments. However, only the noise in case 1 is used to generate the paired “clean/noisy” training patches. In the testing stage, the pairs generated by all the five types of noise are used. The details of the generalization process of noisy HSIs are as follows:

Case 1 (Gaussian + Impulse): Each band in HSI is corrupted with Gaussian noise, and the noise level is randomly selected from [10,70]. The number of selected bands with

additional impulse noise are 10, 10, 40, and 20 for CAVE, ICVL, DC, and PaviaU, respectively. The ratio of impulse noise ranges from [0.1,0.5].

Case 2 (Gaussian + Stripe): All the settings are the same as in Case 1, except that the impulse noise is replaced with the stripe noise. The ratio of the stripe ranges from [0.05,0.2].

Case 3 (Gaussian + Deadline): All the settings are the same as in Case 1, except that the HSI is additionally corrupted with the deadline noise. The ratio of the deadline ranges from [0.05,0.2].

Case 4 (Spatial-Spectral Variant Gaussian): Each band of HSI is corrupted with the spatial-spectral variant Gaussian. The noise level for each band is randomly generated with normal distribution. The range of the noise level is between 10 and 70.

Case 5 (Mixture): The HSIs are corrupted with all the noise types from Case 1 to Case 4.

Four quantitative measures are used to evaluate the denoising performance, i.e., peak signal-to-noise ratio (PSNR), structural similarity (SSIM), spectral angle mapper (SAM), and erreur relative globale adimensionnelle de Synthèse (ERGAS). Adam algorithm is used to optimize the network parameters. The epoch number is set as 10. The initial learning rate is $1e^{-3}$ and decays by a factor 0.8 every epoch. The batch size is set as 10. All the experiments are conducted on a PC with Intel Core i7-8700K CPU, and one GeForce RTX 2080 Ti with 11GB memory.

4.1 Effectiveness test of HWnet

In this section, we conduct experiments to verify the effectiveness of the proposed HWnet, i.e., whether the PnP HWnet can help improve the denoising performance of some popular HSI denoising models. Firstly, the trained HWnet is plugged into three target HSI denoising models, and then we compare them with the existing state-of-the-art HSI denoising methods. Secondly, the HWnet is plugged into the deep image prior (DIP) model, and then we compare the weighted DIP model with the original DIP model.

4.1.1 Compare with Existing Methods

Note that the weighting scheme is an auxiliary part of a weighted denoising model. Then we select HW-LRTV, HW-E3DTV and HW-LRTFDFR as *our* testing methods. The type-‘N+T+TS’ HWnet is used for the three methods. We compare the three methods with several advanced HSI complex noise removal methods including LRMR [11], LRTV [21], NMoG [8], HyRes [64], FastHyMix [33], CTV-RPCA [65], E3DTV [20], LRTFDFR [10], HSI-DeNet [35] and HSI-CNN [36].

The quantitative results are reported in Table 3. From the table, we can easily observe that the PnP HWnet can dramatically improve the denoising results by comparing LRTV with HW-LRTV or by comparing E3DTV with HW-E3DTV. Additionally, it can also be seen that our methods generally perform the best for different types of noise patterns even though only the noise in Case 1 is used in the training process. This verifies that the HWnet can learn a general weight prediction rule for a wide range of noise types and thus can help the weighted model to finely adapt to more noise types. Although FastHyMix achieves the best results in Case 2 (Gaussian+stripe), it does not perform well

²<https://www.cs.columbia.edu/CAVE/databases/multispectral>

³<http://icvl.cs.bgu.ac.il/hyperspectral/>

⁴<https://engineering.purdue.edu/~biehl/MultiSpec/hyperspectral.html>

⁵https://www.ehu.es/ccwintco/index.php/Hyperspectral_Remote_Sensing_Scenes

⁶<https://erdclibrary.erdclib.dren.mil/jspui/handle/11681/2925>

Table 3: Average test performance of different HSI denoising competing methods on the ICVL dataset. The best results in each row are in **bold**, and the second best results in each row are with underline.

noise	index	advanced existing methods										<i>ours</i>		
		LRMR	LRTV	NMoG	HyRes	FastH-yMix	CTV-RPCA	E3DTV	LRTF-DFR	HSI-DeNet	HSI-CNN	HW-LRTV	HW-E3DTV	HW-LR-TDFDR
1	PSNR	24.35	31.67	28.90	30.00	31.09	31.09	<u>34.61</u>	29.69	29.33	34.36	34.94	35.41	34.09
	SSIM	0.7214	0.9059	0.8718	0.8829	0.8914	0.8636	<u>0.9511</u>	0.8376	0.8588	0.9320	0.9495	0.9529	0.9505
2	PSNR	27.77	32.91	30.32	35.09	37.30	30.99	34.27	30.83	28.95	35.65	35.62	35.46	34.44
	SSIM	0.8198	0.9252	0.9088	0.9566	0.9680	0.8579	0.9473	0.8479	0.8389	0.9551	<u>0.9593</u>	0.9590	0.9540
3	PSNR	26.45	31.34	29.09	32.16	<u>34.19</u>	30.37	33.52	27.92	28.39	33.64	34.52	35.20	33.75
	SSIM	0.7962	0.9135	0.9013	0.9308	0.9571	0.8484	0.9425	0.7729	0.8308	0.9456	0.9523	<u>0.9568</u>	0.9464
4	PSNR	26.15	35.49	26.68	32.25	36.23	28.94	32.88	31.52	30.31	37.38	<u>37.00</u>	34.55	35.42
	SSIM	0.7794	0.9543	0.8422	0.9241	0.9610	0.7944	0.9271	0.8553	0.8843	<u>0.9649</u>	0.9692	0.9476	0.9640
5	PSNR	23.00	30.30	24.70	26.84	27.90	28.45	31.63	28.42	28.37	32.02	33.90	33.26	<u>33.43</u>
	SSIM	0.6868	0.8971	0.7553	0.8357	0.8498	0.7923	0.9154	0.8213	0.8420	0.9206	0.9480	0.9346	<u>0.9469</u>

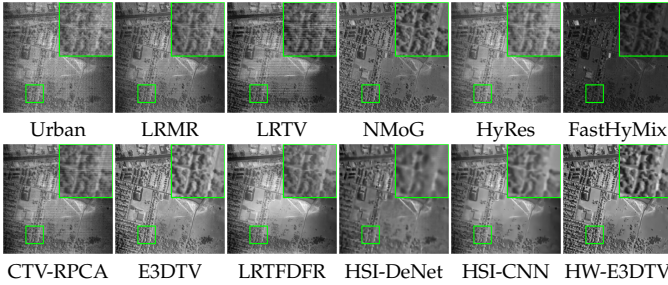


Figure 4: Denoising results by different compared methods on the real noisy HSI Urban.

on the more complex noise in Case 5. We also compare our methods with all competing methods on one real noisy HSI dataset, Urban. The visual comparison is presented in Fig. 4. It can be observed that the restored HSI by our HW-E3DTV method can achieve the best visual result, while other competing methods do not fully remove the noise and the restored HSI always contains obvious blur effects or stripe noise. More experimental results are presented in the supplementary material.

From the above synthetic and real HSI denoising experiments, the effectiveness of our HWnet is reflected in two aspects. First, the PnP HWnet helps boost the denoising performance of traditional HSI denoising models. It should be also noted that the HWnet is not limited to be used on the LRTV, E3DTV and LRTFDFR models, but could be plugged into general weighted HSI denoising models. Second, the HWnet inclines to learn a general weight prediction rule to help a weighted model finely fit a wider range of noise types than those involved in HWNet training.

4.1.2 Deep Image Prior

Except for the traditional denoising models, we further consider the deep image prior (DIP) model for testing. The DIP model is essentially an unsupervised deep learning method that minimizes the distance between the network output and the noisy image. Specifically, the DIP model is formulated as:

$$\min_{\eta} \ell(g_{\eta}(\mathcal{Z}) - \mathcal{Y}) + \lambda R(g_{\eta}(\mathcal{Z})), \quad (10)$$

where $g_{\eta}(\cdot)$ is a deep neural network (DNN) that takes random noise \mathcal{Z} as input and generates the denoised image as output. The network parameters η are to be optimized. The network $g_{\eta}(\cdot)$ needs to be optimized one time for a

given noisy HSI. Once the training is finished (i.e., the optimal parameter η^* is learned), we can immediately obtain the restored image $\hat{\mathcal{X}}$ as $g_{\eta^*}(\mathcal{Z})$. Early DIP works omit the regularization R [66] [67], and recent work [68] adds the term R to bonus the performance and stabilize the training.

Inspired by the aforementioned weighted denoising model, we can also formulate the weighted DIP model as:

$$\min_{\eta} \|\mathcal{W} \odot (g_{\eta}(\mathcal{Z}) - \mathcal{Y})\|_2^2 + \lambda R(g_{\eta}(\mathcal{Z})), \quad (11)$$

where $\mathcal{W} = h_{\theta}(\mathcal{Y})$ is the weight tensor. However, the HWnet for the weighted DIP is barely trainable since the trained network $g_{\eta}(\cdot)$ is only used for one image. Therefore, in this experiment, we directly transfer the seven trained HWnets as described in Table 2 to the weighted DIP model (11). Specifically, we use S2DIP [68] as the backbone model since it is specifically designed for HSI denoising. We modify the S2DIP model as a weighted S2DIP model (HW-S2DIP), and then use this model for HSI denoising.

Table 4 shows the experimental results on the CAVE dataset in five noise cases. Each restoration experiment is repeated 3 times and the average results are recorded. In Table 4, the “max” column presents the maximum output PSNR value during training. The “final” column means the average PSNR values of the last 100 iterations, and also represents the converged results. “|d.v|” is the absolute difference value between the maximum and the final values. From Table 4, we can see that the HW-S2DIP model outperforms the original model in most noise cases. For example, most of the HW-S2DIP models perform better than the original model in the complex noise case (i.e., Case 5). Besides, the “|d.v|” value of the HW-S2DIP model is always smaller than S2DIP, which reveals that the HW-S2DIP models are more stable than the original model. A different observation from previous experiments is that the type-‘T’ HWnet doesn’t perform the worst among all HWnets. This is perhaps due to the extra implicit image prior brought by network g_{η} . Fig. 5 shows the visual comparison of S2DIP and HW-S2DIP in Case 3. We can see that the deadline noise is not completely removed by S2DIP, while most of the HW-S2DIP models achieve better visual results. To illustrate the convergence, we also plot the PSNR tendency during training on Case 3 and Case 5 in Fig. 6. Except for type-‘TS’ HWnet, HW-S2DIP with other HWnets converges very quickly in the early stage. In Case 5, we see that the HW-S2DIP with type-‘N+T+TS’ HWnet suffers from one big vibration at about

Table 4: PSNR results of “jelly_bears” in CAVE dataset for S2DIP and HW-S2DIP with different HWnets. The best results in each **column** are in **bold**, and the second best results in each **column** are with underline.

type	Case 1			Case 2			Case 3			Case 4			Case 5		
	max	final	d.v	max	final	d.v	max	final	d.v	max	final	d.v	max	final	d.v
*Original	31.20	30.91	0.282	31.41	31.18	0.229	30.13	29.89	0.231	33.60	33.44	0.155	30.67	30.43	0.242
N	30.95	30.87	0.074	31.35	31.28	0.076	30.60	30.47	0.137	33.26	33.17	<u>0.092</u>	30.94	30.80	0.145
T	29.85	29.62	0.232	29.63	29.41	0.226	29.50	29.37	0.125	31.18	30.89	0.290	30.31	29.48	0.831
TS	27.94	27.48	0.461	28.90	28.72	0.176	27.96	27.83	0.139	31.05	30.92	0.130	27.72	27.62	<u>0.100</u>
N+T	30.93	30.84	0.088	31.11	31.02	0.087	30.58	30.45	<u>0.123</u>	32.99	32.83	0.165	<u>31.12</u>	31.03	0.092
N+TS	30.46	30.37	0.095	30.85	30.77	0.083	30.35	30.22	0.130	32.94	32.86	0.085	30.74	30.62	0.125
T+TS	31.10	<u>31.02</u>	0.078	<u>31.43</u>	<u>31.34</u>	0.090	<u>30.80</u>	<u>30.67</u>	0.131	33.10	33.00	0.096	31.02	30.90	0.113
N+T+TS	<u>31.16</u>	31.09	<u>0.076</u>	31.54	31.45	<u>0.081</u>	30.87	30.78	0.097	<u>33.48</u>	<u>33.37</u>	0.117	31.33	<u>30.91</u>	0.424

the 6000_{th} iteration, which causes a large “|d.v|” value 0.424 in Table 4. However, its performance keeps rising after the 6000_{th} iteration and finally reaches the third best.

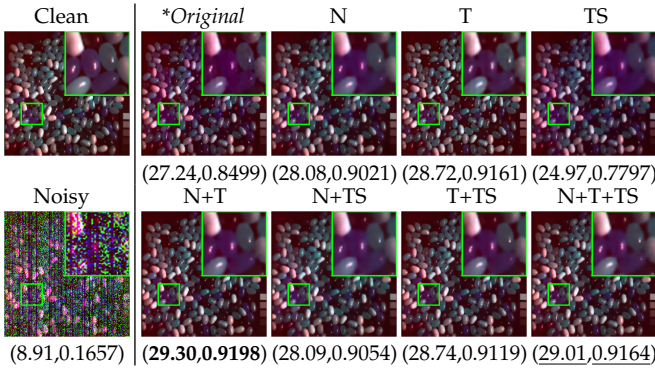


Figure 5: Visual comparison of S2DIP and HW-S2DIP with different HWnets of “jelly_bears” in CAVE dataset. The PSNR and SSIM measures are shown below each restored image for easy observation..

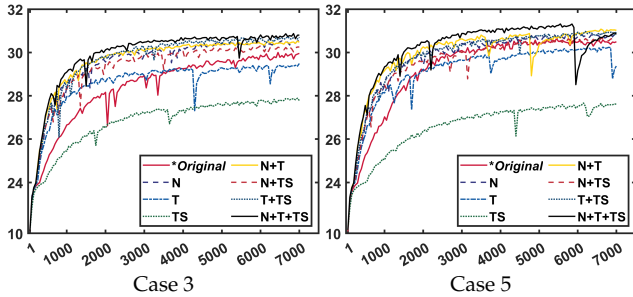


Figure 6: The tendency of PSNR values during iterations for S2DIP and HW-S2DIP with different HWnets.

4.2 Generalization Experiments

In the last section, it is shown that the trained HWnet can be embedded into a weighted denoising model in a PnP manner. In this section, we turn to explore how HWnet can behave between various source and target models.

4.2.1 Synthetic Generalization

In this experiment, we choose the target models exactly from the source models (i.e. HW-NNM, HW-TV, and HW-TVS). Since the divergence between source and target models are relatively clear, we can take a closer look at the generalization ability of all seven HWnets across different models.

The average experimental results on the ICVL dataset are shown in Table 5. The first row describes seven combinations of source models for training HWnet, and the first column represents the different noise types. For example, the “T” column in the target model 1 chart means that the HWnet applied for HW-NNM is trained only using HW-TV and the quantitative results under five noise types are reported. From Table 5, we can also observe that although the HWnet is trained only using the noise in Case 1, it can be finely generalized to other types of noises (Cases 2-5) which have not been seen during training.

Additionally, we compute the average PSNR value of all the five noise cases based on Table 5, and the results are demonstrated in Table 6. Combining the two tables, we have the following observations. First, the corresponding HWnet inclines to perform the best when the source models and the target models match. For example, in Table 5, if the source model is ‘N’, the best denoising performance is obtained when the target model is HW-NNM. The phenomena can also be clearly seen from Table 6 whose diagonal values are the best. Second, the type-‘T’ HWnet does not generalize well to the other two models (i.e., ‘N’ and ‘TS’), while type-‘N’ HWnet generalizes better than the other two types of HWnet. Third, although the inconsistency between source and target models degrades the performance, the performance on the target models is still well enough. Fourth, when the number of source models is more than one, the test performance is obviously better than one source model case since the HWnet can capture more regularization information from multiple source models, which is clearly illustrated in the last column of Table 6. In the next section, we will further understand the above generalization behaviors from the theoretical analysis.

4.2.2 Model Generalization

In this section, we further verify the generalization performance of our proposed HWnet on brand new and more complex target models, which have not been seen during training. Specifically, we select three popular HSI denoising models (i.e., LRTV [21], E3DTV [20], LRTFDFR [10]) that are designed to handle complex noise as the target models. The LRTV [21] is a matrix-based method, which utilizes both spatial smoothness property and spectral low-rank property. The E3DTV [20] is a tensor-based method that explores the sparsity of the base matrix of the gradient map in each mode. The loss functions of LRTV and E3DTV are both ℓ_1 norm. The LRTFDFR [10] employs the spectral low-rankness, the group sparsity on the gradient map of the base

Table 5: Average test performance of HW-NNM, HW-TV and HW-TVS on ICVL dataset. The best results in each row are in **bold**, and the second best results in each row are with underline.

source noise	N	T	TS	N+T	N+TS	T+TS	N+T+TS
	PSNR/SSIM	PSNR/SSIM	PSNR/SSIM	PSNR/SSIM	PSNR/SSIM	PSNR/SSIM	PSNR/SSIM
target model 1 : HW-NNM							
Case 1	<u>33.16</u> / 0.9452	22.44/0.6523	27.38/0.8348	32.53/0.9413	33.31 / <u>0.9440</u>	26.93/0.8292	32.93/0.9434
Case 2	<u>33.60</u> / <u>0.9493</u>	22.31/0.6449	27.80/0.8421	32.95/0.9431	33.71 / 0.9502	26.83/0.8257	33.35/0.9482
Case 3	<u>32.54</u> / 0.9461	22.37/0.6500	26.98/0.8320	31.80/0.9352	32.59 / <u>0.9433</u>	26.51/0.8228	32.16/0.9406
Case 4	32.39 / 0.9267	18.99/0.5332	25.09/0.7592	31.25/0.9138	<u>32.05</u> / <u>0.9253</u>	23.71/0.7321	31.54/0.9215
Case 5	30.43 / 0.9029	19.89/0.5492	23.90/0.7127	29.46/0.8907	<u>29.85</u> / <u>0.8950</u>	23.87/0.7287	29.61/0.8941
target model 2 : HW-TV							
Case 1	29.27/0.8355	32.84 / 0.9274	27.53/0.7872	31.52/0.8894	29.10/0.8343	<u>31.53</u> / <u>0.8898</u>	30.97/0.8757
Case 2	29.40/0.8459	32.95 / 0.9356	27.67/0.7935	<u>31.81</u> / <u>0.8987</u>	29.23/0.8461	31.72/0.8974	31.19/0.8862
Case 3	28.97/0.8385	31.94 / 0.9275	26.75/0.7762	<u>31.03</u> / <u>0.8916</u>	28.82/0.8372	30.76/0.8877	30.60/0.8793
Case 4	28.65/0.8272	31.38 / 0.9087	26.73/0.7695	30.89/0.8807	28.53/0.8283	30.80/0.8804	30.40/0.8697
Case 5	27.58/0.8003	29.67 / 0.8774	25.19/0.7229	<u>29.16</u> / <u>0.8555</u>	27.50/0.7985	28.97/0.8503	28.96/0.8427
target model 3 : HW-TVS							
Case 1	31.26/0.9125	24.17/0.6991	33.22 / 0.9249	30.49/0.9094	<u>32.35</u> / <u>0.9238</u>	32.03/ <u>0.9241</u>	31.77/0.9240
Case 2	31.04/0.9135	23.97/0.6863	33.48 / 0.9292	30.22/0.9065	<u>32.34</u> / <u>0.9267</u>	32.08/0.9257	31.71/0.9253
Case 3	31.30/0.9151	24.05/0.6942	32.85 / <u>0.9243</u>	30.31/0.9060	32.49 / 0.9260	31.59/0.9193	31.73/0.9239
Case 4	29.52/0.8833	21.30/0.5930	32.00 / 0.9041	28.67/0.8733	<u>30.96</u> / <u>0.9018</u>	30.54/0.8957	30.28/0.8981
Case 5	29.59/0.8711	21.88/0.6039	<u>30.47</u> / <u>0.8784</u>	28.59/0.8599	30.60 / 0.8858	29.49/0.8723	29.84/0.8807

Table 6: Average PSNR/SSIM values of all five kinds of noise patterns obtained by HW-NNM, HW-TV and HW-TVS on ICVL dataset. The best results in each column are in **bold**, and the second best results in each column are with underline.

target source	HW-NNM	HW-TV	HW-TVS	HW-NNM & HW-TV	HW-NNM & HW-TVS	HW-TV & HW-TVS	HW-NNM & HW-TV & HW-TVS
N	32.42 / 0.9340	28.77/0.8295	30.54/0.8991	30.60/0.8818	31.48/0.9166	29.66/0.8643	30.58/0.8875
T	21.20/0.6059	31.76 / 0.9153	23.07/0.6553	26.48/0.7606	22.14/0.6306	27.41/0.7853	25.34/0.7255
TS	26.23/0.7962	26.77/0.7699	<u>32.40</u> / <u>0.9122</u>	26.50/0.7830	29.32/0.8542	29.59/0.8410	28.47/0.8261
N+T	31.60/0.9248	<u>30.88</u> / <u>0.8832</u>	29.66/0.8910	31.24 / 0.9040	30.63/0.9079	30.27/0.8871	30.71/0.8997
N+TS	<u>32.30</u> / <u>0.9316</u>	28.64/0.8289	31.75 / 0.9128	30.47/0.8802	32.03 / 0.9222	30.19/0.8709	30.90/0.8911
T+TS	25.57/0.7877	30.75/0.8811	31.14/0.9074	28.16/0.8344	28.36/0.8476	30.95 / 0.8943	29.16/0.8587
N+T+TS	31.92/0.9296	30.42/0.8707	31.07/0.9104	<u>31.17</u> / <u>0.9001</u>	<u>31.49</u> / <u>0.9200</u>	<u>30.75</u> / <u>0.8906</u>	31.14 / 0.9036

Table 7: Average test performance of HW-LRTV, HW-E3DTV and HW-LRTDFR on ICVL dataset. The best results in each row are in **bold**, and the second best results in each row are with underline.

source noise	*Original	N	T	TS	N+T	N+TS	T+TS	N+T+TS
	PSNR/SSIM	PSNR/SSIM	PSNR/SSIM	PSNR/SSIM	PSNR/SSIM	PSNR/SSIM	PSNR/SSIM	PSNR/SSIM
target model 1 : HW-LRTV								
Case 1	31.67/0.9059	34.44/0.9419	28.76/0.8152	31.45/0.9122	34.54 / 0.9503	34.30/0.9417	34.31/0.9416	<u>34.94</u> / <u>0.9495</u>
Case 2	32.91/0.9252	35.23/0.9538	29.23/0.8353	32.73/0.9275	<u>35.41</u> / <u>0.9592</u>	35.06/0.9542	35.05/0.9496	35.62 / 0.9593
Case 3	31.34/0.9135	34.21/0.9476	28.85/0.8301	31.01/0.9179	<u>34.22</u> / <u>0.9531</u>	34.08/0.9462	33.57/0.9435	34.52 / <u>0.9523</u>
Case 4	35.49/0.9543	36.61/0.9645	32.25/0.9145	34.44/0.9520	<u>36.90</u> / <u>0.9709</u>	36.59/0.9658	36.61/0.9686	37.00 / <u>0.9692</u>
Case 5	30.30/0.8971	<u>33.57</u> / <u>0.9418</u>	28.94/0.8346	30.30/0.9102	<u>33.34</u> / <u>0.9467</u>	33.55/0.9426	33.07/0.9432	33.90 / 0.9480
target model 2 : HW-E3DTV								
Case 1	34.61/0.9511	34.97/0.9474	30.34/0.8741	34.37/0.9396	35.16/ 0.9563	34.95/0.9467	<u>35.70</u> / <u>0.9551</u>	<u>35.41</u> / <u>0.9529</u>
Case 2	34.27/0.9473	35.04/0.9532	29.76/0.8571	34.77/0.9474	35.18/ <u>0.9605</u>	35.10/0.9542	35.81 / 0.9613	<u>35.46</u> / <u>0.9590</u>
Case 3	33.52/0.9425	35.06/0.9540	29.59/0.8591	33.53/0.9409	34.63/ 0.9570	<u>35.10</u> / <u>0.9529</u>	34.83/0.9560	35.20 / <u>0.9568</u>
Case 4	32.88/0.9271	34.12/0.9420	27.81/0.7918	33.53/0.9331	34.13/0.9478	34.19/0.9425	34.77 / 0.9492	34.55/0.9476
Case 5	31.63/0.9154	33.21/0.9307	27.75/0.7888	31.15/0.9110	32.61/ <u>0.9337</u>	<u>33.23</u> / <u>0.9300</u>	32.77/0.9318	33.26 / 0.9346
target model 3 : HW-LRTDFR								
Case 1	29.69/0.8376	33.63/0.9421	27.97/0.8116	32.03/0.9224	33.70/ <u>0.9506</u>	33.81/0.9444	34.16 / 0.9526	<u>34.09</u> / <u>0.9505</u>
Case 2	30.83/0.8479	34.21/0.9496	28.66/0.8374	32.82/0.9287	34.17/0.9523	34.03/0.9491	34.56 / <u>0.9525</u>	<u>34.44</u> / <u>0.9540</u>
Case 3	27.92/0.7729	33.25/0.9402	28.29/0.8267	31.25/0.9064	33.10/0.9418	33.37/0.9406	<u>33.43</u> / <u>0.9426</u>	33.75 / 0.9464
Case 4	31.52/0.8553	35.41/0.9617	31.12/0.9096	34.70/0.9534	35.23/ 0.9642	35.23/0.9614	35.51 / <u>0.9630</u>	<u>35.42</u> / <u>0.9640</u>
Case 5	28.42/0.8213	33.00/0.9382	28.41/0.8340	31.61/0.9248	32.70/0.9436	33.22/0.9413	<u>33.22</u> / <u>0.9475</u>	33.43 / <u>0.9469</u>

matrix, and column continuity of the spectral factor matrix. The loss term of LRTDFR includes both weighted ℓ_1 norm and ℓ_2 norm. For each of the three target models, we modify it as the weighted denoising model by simply replacing the loss term with the weighted ℓ_2 loss. For a given noisy HSI

in the test stage, once the weight of the weighted model is calculated by the HWnet, the weighted model can then be solved by the algorithm inherited from the original model. More specifically, the modified HW-LRTV and HW-E3DTV models are optimized by the Augment Lagrange Multiplier

Table 8: Average PSNR/SSIM values of all five kinds of noise patterns obtained by HW-NNM, HW-TV and HW-TVS on ICVL dataset.

target source	HW-LRTV	HW-E3DTV	HW- LRTFDFR
*Original	32.34/0.9192	33.38/0.9367	29.68/0.827
N	34.81/0.9499	34.48/0.9455	33.9/0.9464
T	29.61/0.8459	29.05/0.8342	28.89/0.8439
TS	31.99/0.924	33.47/0.9344	32.48/0.9271
N+T	<u>34.88/0.9560</u>	34.34/0.9511	33.78/0.9505
N+TS	34.72/0.9501	34.51/0.9453	33.93/0.9474
T+TS	34.52/0.9493	<u>34.78/0.9507</u>	34.18/0.9516
N+T+TS	<u>35.20/0.9557</u>	34.78/0.9502	<u>34.23/0.9524</u>

(ALM) method which is also adopted in the original LRTV and E3DTV models. As for the modified HW-LRTFDFR model, we also adopt the ALM algorithm to solve this model because the proximal alternating minimization algorithm can hardly be directly inherited. More algorithm details are presented in the supplemental material.

In this experiment, we apply the seven trained HWnets in the previous Sec. 4 to the HW-LRTV, HW-E3DTV, and HW-LRTFDFR models in a plug-and-play manner. The denoising results on the ICVL dataset are illustrated in Table 7. It should be noted that the first column of each sub-table in Table 7 records the performance of the original LRTV, E3DTV, and LRTFDFR models. Additionally, we also have the following observations from Table 7. Firstly, most weighted models outperform their original models. This should attribute to the powerful complex noise description ability of the weighted ℓ_2 loss. Second, although only ‘‘Gaussian+impulse’’ noise is used for training the HWnet, the weighted denoising model whose weight is predicted by the trained HWnet can also achieve superior results than the original models in other noise cases, which further proves the effectiveness of our HWnet to handle complex noise. This can be rationally explained by that our HWnet has learned the essential noise characteristics from the training data, and thus can be well generalized to other noise types.

Table 8 averages the PSNR/SSIM results of all five noise cases. From Tables 7 and 8, we can observe that for the HW-LRTV model, the type-‘N+T+TS’ and type-‘N+T’ HWnets obtain the best and second best performance, which is reasonable since LRTV mainly considers the low-rankness and spatial smoothness property, complying with the ‘N’ regularization and ‘T’ regularization, respectively. As for HW-E3DTV and HW-LRTFDFR, the last two HWnets achieve the best results, which should attribute to the fact that the HWnet learned from diverse models can generally capture more HSI priors, and thus can generalize well to a wide range of new target models. Additionally, we also notice that the type-‘T’ HWnet gains the lowest performance among the original and other weighted models. The reason might be that the TV regularization only grabs the spatial features while neglects the spectral correlation property, which has been verified to be of great importance for HSI denoising.

Further, Fig. 7 shows the visual comparison of the three new target models and their corresponding weighted models with different HWnets. It can be easily seen that except for type-‘T’ HWnet, the proposed weighted models with other HWnets can effectively remove the complex noise. For type-‘TS’ HWnet, some image details may be lost and the

image always contains blurry boundaries. Additionally, the type-‘N+T+TS’ HWnet can achieve the best visual results.

5 GENERALIZATION THEORY ANALYSIS

In Sec. 4, it has been empirically verified that the HWnet has good generalization ability across diverse noisy HSIs and weighted denoising models. In this section, we turn to explore theoretical analysis to help more essentially interpret the above generalization behavior. Note that our theoretical research mainly focuses on model generalization rather than generalization across HSI datasets. The latter will be further investigated in our future research.

To build the theoretical analysis, we firstly replenish the general multi-model bi-level learning framework introduced in Sec. 3.2.2. Then, we provide a training error estimation to clarify that each HSI denoising model contributes to the final training performance. Next, we prove a generalization error upper bound of our proposed HWnet for illuminating its intrinsic model generalization capability. All proof details are presented in the supplementary material.

5.1 Preparation for Multi-Model Framework

Let data space \mathbb{Y} and \mathbb{X} denote the degraded image space and the clean image space, respectively. We have that $\mathcal{Y} \in \mathbb{Y}$ and $\mathcal{X}_{gt} \in \mathbb{X}$. Denote M as the size index $h * w * b$, and we assume that $\mathbb{Y} \subset \mathbb{R}^M$ and $\mathbb{X} \subset \mathbb{R}^M$. Furthermore, \mathbb{Y} and \mathbb{X} should be considered to be bounded since the clean images are usually normalized in the pre-processing step. Although the additive random noise is unbounded theoretically, the intensity of an observed noisy image \mathcal{Y} should be definitely limited in real cases. Therefore, we assume that both \mathbb{Y} and \mathbb{X} are bounded sets in \mathbb{R}^M , which is summarized as follows:

Assumption 1. $|\mathcal{Y}| \leq B_d, |\mathcal{X}| \leq B_d, \forall \mathcal{Y} \in \mathbb{Y}, \forall \mathcal{X} \in \mathbb{X}$.

Let D represent a joint distribution defined on $\mathbb{Y} \times \mathbb{X}$. To be specific, the joint probability density function (PDF) $p(\mathcal{Y}, \mathcal{X})$ can usually be decomposed as

$$p(\mathcal{Y}, \mathcal{X}) = p(\mathcal{Y}|\mathcal{X})p(\mathcal{X}), \quad (12)$$

where $p(\mathcal{X})$ represents the PDF of the clean data \mathcal{X} , and $p(\mathcal{Y}|\mathcal{X})$ reveals the generative process of noisy data \mathcal{Y} conditioned on \mathcal{X} ⁷. The training data $(\mathcal{Y}_i, \mathcal{X}_{gt_i})$ are i.i.d sampled from D for all $i \in [N]$.

We firstly prove a Lemma that clarifies the implicit mapping from \mathcal{W} to $\hat{\mathcal{X}}$ as follows.

Lemma 1. *Suppose $\mathcal{W} \geq \varepsilon > 0$ and R is a proper closed and convex function, and then the solution to problem (3) is unique.*

Based on Lemma 1, we can also define the solution of Eq. (3) explicitly as follows:

$$f_{\lambda R}^h(\mathcal{Y}; \theta) := \arg \min_{\mathcal{X}} \frac{1}{2} \|h_{\theta}(\mathcal{Y}) \odot (\mathcal{Y} - \mathcal{X})\|_2^2 + \lambda R(\mathcal{X}), \quad (13)$$

which has an equivalent meaning to $\hat{\mathcal{X}}(\mathcal{Y}, \theta)$. We continue to call ‘‘ $f_{\lambda R}^h$ ’’ a source task. The T source tasks $\{f_{\lambda_t R_t}^h\}_{t=1}^T$ in the lower level problem can be aggregated into

$$\mathcal{F}_{\mathcal{H}} := \{(f_{\lambda_1 R_1}^h, \dots, f_{\lambda_T R_T}^h) | h \in \mathcal{H}\}. \quad (14)$$

⁷Here, we do not distinguish the variable ‘‘ \mathcal{X} ’’ from a sample ‘‘ \mathcal{X} ’’.

	Clean	Noisy	*Original	N	T	TS	N+T	N+TS	T+TS	N+T+TS
LRTV										
	Band 18	(12.05,0.2354)	(30.32,0.8981)	(32.45,0.9153)	(28.77,0.8712)	(31.11,0.9163)	(32.28,0.9403)	(31.58,0.8925)	(32.76,0.9418)	(32.60,0.9179)
E3DTV										
	Band 5	(14.86,0.3510)	(33.91,0.9480)	(36.54,0.9153)	(31.16,0.8764)	(34.60,0.9604)	(35.73,0.9672)	(36.38,0.9657)	(35.93,0.9669)	(36.73,0.9676)
LRTEDFR										
	Band 5	(13.17,0.2346)	(34.42,0.9500)	(34.78,0.9710)	(26.77,0.7226)	(32.68,0.9587)	(34.71,0.9729)	(34.57,0.9707)	(35.00,0.9719)	(35.27,0.9754)

Figure 7: Denoising results of different HWNet models on ICVL dataset. From top to bottom, noisy HSIs are corrupted with “Gaussian+impulse”, “mixture” and “Gaussian+deadline” noise patterns.

We call $\mathcal{F}_{\mathcal{H}}$ the source task set since it includes all denoising tasks for training h_{θ} . \mathcal{H} is the hypothesis set that contains all possible h_{θ} captured by θ . Despite the distinction of denoising tasks in $\mathcal{F}_{\mathcal{H}}$, the purposes of weighting are the same, i.e. leveraging noise information for better denoising. In Sec. 5.2, we first analyze the training error. Further, we will discuss the generalization ability of h_{θ} trained from the general bi-level framework as presented in (9a)-(9b).

5.2 Training Error Estimation

Since $\hat{\mathcal{X}}_{ti} = f_{\lambda_t R_t}^h(\mathcal{Y}_{ti})$, the upper level problem (9a) can be equivalently written as

$$\min_{h \in \mathcal{H}} \frac{1}{T} \sum_{t=1}^T \frac{1}{N_t} \sum_{i=1}^{N_t} \ell_{net} \left(f_{\lambda_t R_t}^h(\mathcal{Y}_{ti}), \mathcal{X}_{gt_{ti}} \right). \quad (15)$$

The above objective function now seems to be a single loss function. However, remember that $f_{\lambda R}^h(\cdot)$ takes an implicit form as the solution to an optimization problem. Also, it is obviously seen that Eq. (15) can be regarded as the empirical risk minimization (ERM) [69] of $h \in \mathcal{H}$ on samples $\mathbf{S} = \{(\mathcal{Y}_{ti}, \mathcal{X}_{gt_{ti}})\}_{i=1}^{N_t} \}_{t=1}^T$. Therefore, our training loss, or empirical risk, refers to

$$\hat{\mathbf{R}}_{tr}(h) := \frac{1}{T} \sum_{t=1}^T \frac{1}{N_t} \sum_{i=1}^{N_t} \ell_{net} \left(f_{\lambda_t R_t}^h(\mathcal{Y}_{ti}), \mathcal{X}_{gt_{ti}} \right). \quad (16)$$

And the expected risk is

$$\mathbf{R}_{tr}(h) := \frac{1}{T} \sum_{t=1}^T \mathbb{E}_{(\mathcal{Y}, \mathcal{X}) \sim \mathcal{D}} \left[\ell_{net} \left(f_{\lambda_t R_t}^h(\mathcal{Y}), \mathcal{X} \right) \right]. \quad (17)$$

The expected risk takes expectations over joint distribution \mathcal{D} . Correspondingly, the “best HWnet”s are defined as:

$$\hat{h}_{tr} := \arg \min_{h \in \mathcal{H}} \hat{\mathbf{R}}_{tr}(h), \quad (18)$$

$$h_{tr}^* := \arg \min_{h \in \mathcal{H}} \mathbf{R}_{tr}(h), \quad (19)$$

where \hat{h}_{tr} is the final trained HWnet under the bi-level framework (9a)-(9b) with a finite set of training samples, and h_{tr}^* is the ideal HWnet which is calculated from the

underlying sample distribution from \mathcal{D} . Since the expected h_{tr}^* is intractable, the training error \mathbf{E}_{tr} to measure the “closeness” between \hat{h}_{tr} and h_{tr}^* is then defined as:

$$\mathbf{E}_{tr} := \mathbf{R}_{tr}(\hat{h}_{tr}) - \mathbf{R}_{tr}(h_{tr}^*). \quad (20)$$

Next, our goal is to estimate the upper bound of \mathbf{E}_{tr} . To achieve this goal, we first need to present some properties and assumptions on the hypothesis set \mathcal{H} and training task set $\mathcal{F}_{\mathcal{H}}$, which is shown as follows:

Lemma 2. Let $h_1, h_2 \in \mathbb{R}^M$ and $0 < \varepsilon \leq h_1, h_2 \leq B_H$. R is convex and closed, and has subgradients. Then $\forall \mathcal{Y} \in \mathbb{Y}$, we have

$$\|f_R^{h_1}(\mathcal{Y}) - f_R^{h_2}(\mathcal{Y})\|_2 \leq L_H \|h_1 - h_2\|_2. \quad (21)$$

The Lipschitz constant L_H only depends on B_d, ε and B_H .

Lemma 2 shows the Lipschitz continuity of a task f_R^h w.r.t weight h , which means that if two input weights h_1 and h_2 are close enough, the corresponding restored images $f_R^{h_1}(\mathcal{Y})$ and $f_R^{h_2}(\mathcal{Y})$ are also close. Additionally, a mild assumption is made on \mathcal{H} , which is shown as

Assumption 2. $0 < \varepsilon \leq h \leq B_H, \forall h \in \mathcal{H}$.

Based on Lemma 2 and Assumption 2, we can decouple the complexity of $\mathcal{F}_{\mathcal{H}}$ by means of the complexity of \mathcal{H} via an analogous chain rule [70]. Similar to [56], the loss ℓ_{net} obeys the following assumption.

Assumption 3. The loss function ℓ_{net} satisfies $|\ell_{net}(\cdot, \cdot)| \leq B_l$ and $\ell_{net}(\cdot, \mathcal{X})$ is L_n -Lipschitz for all $\mathcal{X} \in \mathbb{X}$.

For example, the mean squared error (MSE) $\frac{1}{M} \|\hat{\mathcal{X}} - \mathcal{X}\|^2$ is bounded by $4B_d^2$ and is $\frac{4B_d^2}{\sqrt{M}}$ -Lipschitz about the first input for all $\mathcal{X} \in \mathbb{X}$. Now, we present our main conclusion about the training error \mathbf{E}_{tr} .

Theorem 1. Suppose Assumptions 1, 2 and 3 hold. $\{R_t\}_{t=1}^T$ are convex and closed, and have subgradients. Then, for any $\delta > 0$, with probability at least $1 - \delta$, we have

$$\mathbf{E}_{tr} \leq 6L_n L_H \hat{\mathbf{G}}_S(\mathcal{H}) + \frac{6B_l}{T} \sqrt{\sum_{t=1}^T \frac{1}{N_t}} \sqrt{\frac{\log \frac{2}{\delta}}{2}}. \quad (22)$$

The first term of Eq. (22) is about the Gaussian complexity of \mathcal{H} . Note that elements in our source task set $\mathcal{F}_{\mathcal{H}}$ change with respect to weight net h . This term naturally implies that the more complex \mathcal{H} is, the more uncertainty the training process would bring in about \hat{h}_{tr} . The second term of Eq. (22) is mainly about the size of the training data set S and δ . If we raise the value of $1 - \delta$ such that Eq. (22) is more probable, the value of $\sqrt{\frac{1}{2} \log \frac{2}{\delta}}$ would be higher. Then, to lower the second term, we should enlarge the size of S , i.e. collect more training data. Besides, if one denoising task lacks training samples, the insufficient training of h brought by this task would degrade the joint training performance, even if we increase the training samples for other denoising tasks. This could also be quantified by seeing that $\sqrt{\sum_{t=1}^T \frac{1}{N_t}}$ is the aggregation of $1/N_t$ for all $t \in [T]$. Therefore, we can see that each denoising task contributes to the final training performance.

5.3 Generalization Error Estimation

As aforementioned, transferring the trained HWnet \hat{h}_{tr} to a new weighted denoising model is straightforward since the weight predicted by HWnet contains intrinsic noise features of the observed image. This can be guaranteed owing to our explicit weighting mechanism (i.e., HWnet). For one new weighted denoising model (i.e., target model),

$$\min_{\mathcal{X}} \frac{1}{2} \|\mathcal{W} \odot (\mathcal{Y} - \mathcal{X})\|_2^2 + \lambda_t R_t(\mathcal{X}) \quad (t \geq T + 1), \quad (23)$$

retraining another HWnet in the bi-level learning framework (9a)-(9b) is time-consuming. Fortunately, it is very convenient to apply the off-the-shelf \hat{h}_{tr} in a PnP manner.

More importantly, two tough situations are probably to occur when we begin to train a new HWnet. Firstly, most algorithms require many steps to converge. Besides, solving the subproblems included in the optimization process also needs extra iterative updating and thus results in a large amount of updating steps in total. Since the updating results in each step need to be stored, the demand for the computational resource inclines also to be large. Furthermore, the cumbersome computation graph would make the training of the network inefficient. Secondly, the algorithm to solve the weighted denoising model (23) may involve nondifferentiable operators, e.g., searching non-local similar patches within a single image requires a nondifferential clustering step [29] [15] [27], which makes the training challenging.

Therefore, it is significative to transferably use \hat{h}_{tr} to other denoising models. Under the bi-level framework (9a)-(9b), different denoising models in the lower level optimization problem would generate different HWnets. As aforementioned, the transferability of HWnet comes from the common intrinsic noise property contained in different denoising models. However, any denoising models can not obtain the ideal restored image $\hat{\mathcal{X}}$, namely $\hat{\mathcal{X}} = \mathcal{X}_{gt}$. We regard the imperfect recovery performance as the defects of the denoising model. Further, we assume that these defects come from the regularization term. Consequently, the HWnet learned from multiple source denoising models would additionally compensate the fitting ability between $\hat{\mathcal{X}}$ and \mathcal{X}_{gt} for regularization terms. To be specific, the upper level problem tries to fit the minimum point $\hat{\mathcal{X}}$ of

the lower level problem to the ground-truth image \mathcal{X}_{gt} . However, the distribution of \mathcal{X}_{gt} (i.e., $p(\mathcal{X}_{gt})$) is irrelevant to a specific denoising model in the low level problem. Therefore, there exists some improvement space to fit $p(\mathcal{X}_{gt})$. This space reveals what we call task divergence from the other hand. During training, different denoising models (i.e., those with different regularization terms) can generate different HWnets, which tends to be beneficial to fill up such space. Since each denoising model has its own "best HWnet", transferring a learned \hat{h}_{tr} would naturally bring in generalization error. Next, we will discuss this error in detail from the view of task divergence.

First, similar to the training error, we establish the test error for S target models (23) as:

$$\mathbf{R}_{te}(h) := \frac{1}{S} \sum_{t=T+1}^{T+S} \mathbb{E}_{(\mathcal{Y}, \mathcal{X}) \sim \mathcal{D}} \left[\ell_{net} \left(f_{\lambda_t R_t}^h(\mathcal{Y}), \mathcal{X} \right) \right], \quad (24)$$

where $\{R_t\}_{t=T+1}^{T+S}$ is usually different from $\{R_t\}_{t=1}^T$. The corresponding "best" HWnet for the new model can then be defined as:

$$h_0^* = \arg \min_{h \in \mathcal{H}} \mathbf{R}_{te}(h). \quad (25)$$

The generalization error is thus defined as:

$$\mathbf{E}_g := \mathbf{R}_{te}(\hat{h}_{tr}) - \mathbf{R}_{te}(h_0^*), \quad (26)$$

where $\mathbf{R}_{te}(\hat{h}_{tr})$ represents the test error on the trained HWnet, and $\mathbf{R}_{te}(h_0^*)$ is the test error infimum on the hypothesis set \mathcal{H} . To estimate \mathbf{E}_g , our main challenge relies on measuring the divergence between the source and target tasks, i.e., calculating $\mathbf{R}_{te}(h) - \mathbf{R}_{tr}(h)$. More related analysis details are presented in the supplemental material.

The major difficulty of calculating $\mathbf{R}_{te}(h) - \mathbf{R}_{tr}(h)$ comes from the implicit form of $f_{\lambda R}^h$. We thus seek an approximation of $f_{\lambda R}^h$ to ease the calculation by means of the modified gradient step [71]. Specifically, suppose R is differentiable, by taking the derivative of the objective function in Eq. (13) with respect to \mathcal{X} , the solution $\hat{\mathcal{X}}$ should satisfy:

$$h^2 \odot (\hat{\mathcal{X}} - \mathcal{Y}) + \lambda \nabla R(\hat{\mathcal{X}}) = 0, \quad (27)$$

$$\Rightarrow \hat{\mathcal{X}} = \left(\mathbf{I} + \frac{\lambda}{h^2} \odot \nabla R \right)^{-1} (\mathcal{Y}), \quad (28)$$

where \mathbf{I} represents the identity mapping. The operator $(\mathbf{I} + g)^{-1}$ is known as the resolvent operator [72]. If g is nonlinear, its resolvent form is still implicit and difficult to analyze. Therefore, we approximate Eq. (28) by using a linear transform to ∇R [71] [72]:

$$\left(\mathbf{I} + \frac{\lambda}{h^2} \odot \nabla R \right)^{-1} \approx \mathbf{I} - \frac{\lambda}{h^2} \odot \nabla R. \quad (29)$$

The residual part of such approximation is $o(\lambda/h^2)$ as λ/h^2 goes to 0. In the rest of this section, we analyze the generalization error using the approximated form of $f_{\lambda R}^h$ as

$$\bar{f}_{\lambda R}^h = \mathbf{I} - \frac{\lambda}{h^2} \odot \nabla R. \quad (30)$$

It is easy to verify that $\bar{f}_{\lambda R}^h$ is \bar{L}_H -Lipschitz with respect to h . By utilizing Eq. (30), we firstly present a lemma to estimate $|\mathbf{R}_{te}(h) - \mathbf{R}_{tr}(h)|$.

Lemma 3. Suppose that the function $\bar{f}_{\lambda R}^h$ takes the form of $\mathbf{I} - \frac{\lambda}{h^2} \odot \nabla R$ and ℓ_{net} is MSE loss. For any $h \in \mathcal{H}$, we have

$$|\mathbf{R}_{te}(h) - \mathbf{R}_{tr}(h)| \leq \mathbb{E}_{(\mathcal{Y}, \mathcal{X}) \sim \mathcal{D}} \left\{ \frac{4B_d}{\sqrt{M\varepsilon}} A_1 + \frac{1}{M\varepsilon^2} A_2 \right\},$$

where

$$A_1 = \left\| \left(\frac{1}{T} \sum_{t=1}^T \lambda_t \nabla R_t - \frac{1}{S} \sum_{t=T+1}^{T+S} \lambda_t \nabla R_t \right) (\mathcal{Y}) \right\|_2, \quad (31)$$

$$A_2 = \left| \frac{1}{T} \sum_{t=1}^T \|(\lambda_t \nabla R_t) (\mathcal{Y})\|_2^2 - \frac{1}{S} \sum_{t=T+1}^{T+S} \|(\lambda_t \nabla R_t) (\mathcal{Y})\|_2^2 \right|. \quad (32)$$

We see that Lemma 3 presents the task divergence by evaluating the regularization gradient. This is because we approximate $f_{\lambda R}^h$ by $\bar{f}_{\lambda R}^h$. The first term A_1 compares an average difference of regularization gradients between all source and target tasks, while the second term A_2 compares such average source-target difference in terms of the norms of their regularization gradients.

Based on Lemma 3, we can directly estimate the generalization error \mathbf{E}_g as follows.

Theorem 2. Suppose that Assumptions 1, 2 and 3 hold, $\{R_t\}_{t=0}^T$ are convex and closed, $\bar{f}_{\lambda R}^h$ takes the form of $\mathbf{I} - \frac{\lambda}{h^2} \odot \nabla R$, and ℓ_{net} is MSE loss. Then for any $\delta > 0$, with probability at least $1 - \delta$, we have

$$\mathbf{E}_g \leq 6L_n \bar{L}_H \hat{\mathfrak{G}}_S(\mathcal{H}) + \frac{6B_l}{T} \sqrt{\sum_{t=1}^T \frac{1}{N_t}} \sqrt{\frac{\log \frac{2}{\delta}}{2}} + \mathbb{E}_{(\mathcal{Y}, \mathcal{X}) \sim \mathcal{D}} \left\{ \frac{8B_d}{\sqrt{M\varepsilon}} A_1 \right\} + \mathbb{E}_{(\mathcal{Y}, \mathcal{X}) \sim \mathcal{D}} \left\{ \frac{2}{M\varepsilon^2} A_2 \right\}, \quad (33)$$

where A_1 takes the form of (31) and A_2 of (32).

The upper bound in (33) mainly contains two parts. The first leading two terms represent the aforementioned training error upper bound in Theorem 1, which constrains the distance between \hat{h}_{tr} and h_{tr}^* and reveals how well \hat{h}_{tr} is learned. The rest two terms are the main part to evaluate the generalization error since they measure the diversity between the source and target tasks according to Lemma 3. And our main focus is on analyzing A_1 and A_2 . It can be seen that both terms bound \mathbf{E}_g by expecting on average difference of regularization gradients between the source and target tasks for evaluating the overall source-target divergence.

Now we look back to Table 6. The diagonal results are generally the best since the source and target tasks exactly match. For a single target task, let us take the first column of Table 6 as an example where the target model is HW-NNM. The test performance order of HWnet for a single source task is ‘N’ > ‘TS’ > ‘T’. As we add more source tasks, the behavior is ‘N+TS’ > ‘N+T’ > ‘T+TS’ and seems consistent with single source task behavior. One exception is for target tasks ‘HW-TV&HW-TVS’, where we find that the performance of HWnet with single source model ‘N’ is better than that with ‘TS’ while type-‘T+TS’ HWnet is still better than type-‘N+T’ HWnet. It should be indicated that besides the intrinsics revealed by our learning theory, which should be inspiring to understand the insightful working mechanism underlying

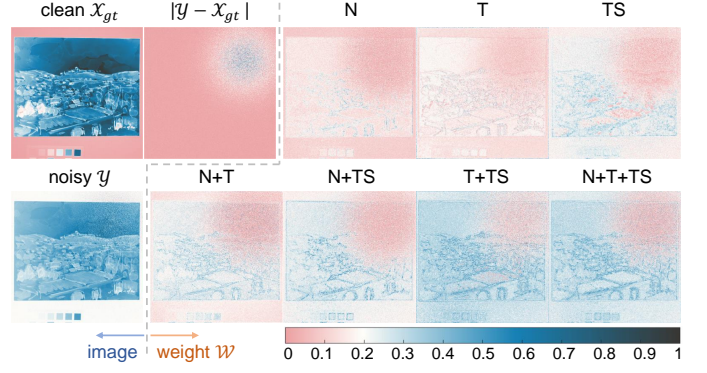


Figure 8: Visual comparison of weight \mathcal{W} s predicted by different types of HWnet.

our method, especially for its generalization ability, some other practical factors could also affect the generalization behavior, such as training effectiveness. This is similar to the roles of the conventional learning theory results. Please see more related theoretical analysis and proof details on Theorem 2 in the supplemental material.

6 DISCUSSION

6.1 Weight Visualization

It is evident that the implementation principle of HWNet is to extract a shared explicit weighting scheme across different noisy HSIs and diverse source models. This rationally makes it capable of capturing a unified weighting policy for general noisy HSIs with diverse noise types and different source models with diverse regularization terms. This implies that the extracted weight mapping from the trained HWNet for a testing HSI should beneficially deliver both its contained noise information and its possessed structural prior knowledge. To intuitively illustrate this capability of HWNet, from the results of Sec. 4.2.2, we visualize the predicted weight calculated by the trained HWnet on a typical testing HSI in Fig. 8.

In this visualization experiment, one band of the ‘watercolor’ image in the CAVE dataset is corrupted with spatially non-i.i.d Gaussian noise, and the top-right area of the image is more heavily corrupted than the remaining areas. The clean image, noisy image, the absolute value of the additive noise, and the weights predicted by the seven types of HWnets are visualized in Fig. 8. From the figure, the aforementioned analysis can be finely validated. Firstly, the heavy noise information located in the top-right area can be recognized by the weight mappings predicted by all trained HWnets. The weight values in this noisy area are very small, meaning that HWNet recognizes this polluted area and attempts to suppress its negative influence on the recovery by setting relatively smaller weights on it. Secondly, all outputted weights from HWNet show evident structural shapes consistent with that of the groundtruth clean image. Especially, more important image structures for recovery, e.g., edges and textures, have been more emphasized by HWNet through specifying larger weights on them. Such a proper weighting manner then naturally conducts its fine HSI denoising effects for the proposed HWNet method through our experiments.

6.2 Limitations

The proposed automatic weighting scheme still has several limitations. Firstly, the learning of the HWnet requires the iterative optimization algorithm of solving the lower level problem to be differentiable. However, some common operators only have sub-gradients, such as nuclear norm and total variation (TV) norm, which tends to make the training of HWnet unstable. Secondly, the theoretical analysis of generalization error is based on an approximation to the source model. Besides, the source and target tasks are symmetric in Lemma 3, while in practice it could be different when exchanging the source and target tasks. Thus there still exists some gap in fully understanding the generalization behavior of HWnet. Additionally, how to further improve the generalization ability of HWnet still needs to be more deeply and comprehensively investigated. Some possible strategies may help, like adding regularizations to the predicted values in the training loss ℓ_{net} [34] or constraining specific structures on the predicted parameters [57]. We will investigate these issues in our future research.

7 CONCLUSION

In this work, we have proposed an automatic weighting scheme for the weighted HSI denoising models. The weight is predicted by an explicit neural network mapping called HWnet, which can be learned under a bi-level optimization framework. The trained HWnet has been validated to be able to generalize to other weighted HSI denoising models in a plug-and-play manner. Experimental results have substantiated that the proposed HWnet can help a testing weighted model to finely adapt to complex noise types, and thus can generalize well to different HSI datasets. Also, our experiments also have validated that the HWnet can be used for new weighted models with diverse regularizers to improve their denoising performance. Additionally, we have further theoretically proved a generalization error upper bound of the HWnet when it is plugged into a new weighted denoising model, showing its insightfully possessed generalization capability.

REFERENCES

- [1] D. G. Manolakis, R. B. Lockwood, and T. W. Cooley, *Hyperspectral Imaging Remote Sensing: Physics, Sensors, and Algorithms*. Cambridge University Press, 2016.
- [2] B. Lu, P. D. Dao, J. Liu, Y. He, and J. Shang, "Recent advances of hyperspectral imaging technology and applications in agriculture," *Remote Sensing*, vol. 12, no. 16, p. 2659, 2020.
- [3] D. Liu, D.-W. Sun, and X.-A. Zeng, "Recent advances in wavelength selection techniques for hyperspectral image processing in the food industry," *Food and Bioprocess Technology*, vol. 7, no. 2, pp. 307–323, 2014.
- [4] J. Pyo, H. Duan, S. Baek, M. S. Kim, T. Jeon, Y. S. Kwon, H. Lee, and K. H. Cho, "A convolutional neural network regression for quantifying cyanobacteria using hyperspectral imagery," *Remote Sensing of Environment*, vol. 233, p. 111350, 2019.
- [5] B. Rasti, P. Scheunders, P. Ghamisi, G. Licciardi, and J. Chanussot, "Noise reduction in hyperspectral imagery: Overview and application," *Remote Sensing*, vol. 10, no. 3, p. 482, 2018.
- [6] D. Meng and F. De La Torre, "Robust matrix factorization with unknown noise," in *Proceedings of the IEEE International Conference on Computer Vision*, 2013, pp. 1337–1344.
- [7] X. Cao, Q. Zhao, D. Meng, Y. Chen, and Z. Xu, "Robust low-rank matrix factorization under general mixture noise distributions," *IEEE Transactions on Image Processing*, vol. 25, no. 10, pp. 4677–4690, 2016.
- [8] Y. Chen, X. Cao, Q. Zhao, D. Meng, and Z. Xu, "Denoising hyperspectral image with non-iid noise structure," *IEEE Transactions on Cybernetics*, vol. 48, no. 3, pp. 1054–1066, 2017.
- [9] Z. Yue, D. Meng, Y. Sun, and Q. Zhao, "Hyperspectral image restoration under complex multi-band noises," *Remote Sensing*, vol. 10, no. 10, p. 1631, 2018.
- [10] Y.-B. Zheng, T.-Z. Huang, X.-L. Zhao, Y. Chen, and W. He, "Double-factor-regularized low-rank tensor factorization for mixed noise removal in hyperspectral image," *IEEE Transactions on Geoscience and Remote Sensing*, vol. 58, no. 12, pp. 8450–8464, 2020.
- [11] H. Zhang, W. He, L. Zhang, H. Shen, and Q. Yuan, "Hyperspectral image restoration using low-rank matrix recovery," *IEEE Transactions on Geoscience and Remote Sensing*, vol. 52, no. 8, pp. 4729–4743, 2013.
- [12] W. He, H. Zhang, L. Zhang, and H. Shen, "Hyperspectral image denoising via noise-adjusted iterative low-rank matrix approximation," *IEEE Journal of Selected Topics in Applied Earth Observations and Remote Sensing*, vol. 8, no. 6, pp. 3050–3061, 2015.
- [13] Y. Chen, Y. Guo, Y. Wang, D. Wang, C. Peng, and G. He, "Denoising of hyperspectral images using nonconvex low rank matrix approximation," *IEEE Transactions on Geoscience and Remote Sensing*, vol. 55, no. 9, pp. 5366–5380, 2017.
- [14] J. Xue, Y. Zhao, W. Liao, and J. C.-W. Chan, "Nonlocal low-rank regularized tensor decomposition for hyperspectral image denoising," *IEEE Transactions on Geoscience and Remote Sensing*, vol. 57, no. 7, pp. 5174–5189, 2019.
- [15] Q. Xie, Q. Zhao, D. Meng, and Z. Xu, "Kronecker-basis-representation based tensor sparsity and its applications to tensor recovery," *IEEE Transactions on Pattern Analysis and Machine Intelligence*, vol. 40, no. 8, pp. 1888–1902, 2017.
- [16] Y. Chen, W. He, N. Yokoya, T.-Z. Huang, and X.-L. Zhao, "Nonlocal tensor-ring decomposition for hyperspectral image denoising," *IEEE Transactions on Geoscience and Remote Sensing*, vol. 58, no. 2, pp. 1348–1362, 2019.
- [17] J. Lin, T.-Z. Huang, X.-L. Zhao, T.-X. Jiang, and L. Zhuang, "A tensor subspace representation-based method for hyperspectral image denoising," *IEEE Transactions on Geoscience and Remote Sensing*, vol. 59, no. 9, pp. 7739–7757, 2020.
- [18] Q. Yuan, L. Zhang, and H. Shen, "Hyperspectral image denoising employing a spectral-spatial adaptive total variation model," *IEEE Transactions on Geoscience and Remote Sensing*, vol. 50, no. 10, pp. 3660–3677, 2012.
- [19] H. K. Aggarwal and A. Majumdar, "Hyperspectral image denoising using spatio-spectral total variation," *IEEE Geoscience and Remote Sensing Letters*, vol. 13, no. 3, pp. 442–446, 2016.
- [20] J. Peng, Q. Xie, Q. Zhao, Y. Wang, L. Yee, and D. Meng, "Enhanced 3dtv regularization and its applications on hsi denoising and compressed sensing," *IEEE Transactions on Image Processing*, vol. 29, pp. 7889–7903, 2020.
- [21] W. He, H. Zhang, L. Zhang, and H. Shen, "Total-variation-regularized low-rank matrix factorization for hyperspectral image restoration," *IEEE Transactions on Geoscience and Remote Sensing*, vol. 54, no. 1, pp. 178–188, 2015.
- [22] Y. Wang, J. Peng, Q. Zhao, Y. Leung, X.-L. Zhao, and D. Meng, "Hyperspectral image restoration via total variation regularized low-rank tensor decomposition," *IEEE Journal of Selected Topics in Applied Earth Observations and Remote Sensing*, vol. 11, no. 4, pp. 1227–1243, 2017.
- [23] C. Jiang, H. Zhang, L. Zhang, H. Shen, and Q. Yuan, "Hyperspectral image denoising with a combined spatial and spectral weighted hyperspectral total variation model," *Canadian Journal of Remote Sensing*, vol. 42, no. 1, pp. 53–72, 2016.
- [24] T. Lu, S. Li, L. Fang, Y. Ma, and J. A. Benediktsson, "Spectral-spatial adaptive sparse representation for hyperspectral image denoising," *IEEE Transactions on Geoscience and Remote Sensing*, vol. 54, no. 1, pp. 373–385, 2015.
- [25] W. Wei, L. Zhang, C. Tian, A. Plaza, and Y. Zhang, "Structured sparse coding-based hyperspectral imagery denoising with intracluster filtering," *IEEE Transactions on Geoscience and Remote Sensing*, vol. 55, no. 12, pp. 6860–6876, 2017.
- [26] Y.-Q. Zhao and J. Yang, "Hyperspectral image denoising via sparse representation and low-rank constraint," *IEEE Transactions on Geoscience and Remote Sensing*, vol. 53, no. 1, pp. 296–308, 2014.
- [27] Y. Chang, L. Yan, and S. Zhong, "Hyper-laplacian regularized unidirectional low-rank tensor recovery for multispectral image

- denoising," in *Proceedings of the IEEE Conference on Computer Vision and Pattern Recognition*, 2017, pp. 4260–4268.
- [28] W. He, Q. Yao, C. Li, N. Yokoya, Q. Zhao, H. Zhang, and L. Zhang, "Non-local meets global: An integrated paradigm for hyperspectral image restoration," *IEEE Transactions on Pattern Analysis and Machine Intelligence*, 2020.
- [29] S. Gu, Q. Xie, D. Meng, W. Zuo, X. Feng, and L. Zhang, "Weighted nuclear norm minimization and its applications to low level vision," *International Journal of Computer Vision*, vol. 121, no. 2, pp. 183–208, 2017.
- [30] Y. Ma, C. Li, X. Mei, C. Liu, and J. Ma, "Robust sparse hyperspectral unmixing with $\ell_{2,1}$ norm," *IEEE Transactions on Geoscience and Remote Sensing*, vol. 55, no. 3, pp. 1227–1239, 2016.
- [31] E. J. Candes, M. B. Wakin, and S. P. Boyd, "Enhancing sparsity by reweighted ℓ_1 minimization," *Journal of Fourier Analysis and Applications*, vol. 14, no. 5, pp. 877–905, 2008.
- [32] T.-X. Jiang, L. Zhuang, T.-Z. Huang, X.-L. Zhao, and J. M. Bioucas-Dias, "Adaptive hyperspectral mixed noise removal," *IEEE Transactions on Geoscience and Remote Sensing*, vol. 60, pp. 1–13, 2021.
- [33] L. Zhuang and M. K. Ng, "Fasthymix: Fast and parameter-free hyperspectral image mixed noise removal," *IEEE Transactions on Neural Networks and Learning Systems*, pp. 1–15, 2021.
- [34] X. Rui, X. Cao, Q. Xie, Z. Yue, Q. Zhao, and D. Meng, "Learning an explicit weighting scheme for adapting complex hsi noise," in *Proceedings of the IEEE Conference on Computer Vision and Pattern Recognition*, 2021, pp. 6739–6748.
- [35] Y. Chang, L. Yan, H. Fang, S. Zhong, and W. Liao, "Hsi-denet: Hyperspectral image restoration via convolutional neural network," *IEEE Transactions on Geoscience and Remote Sensing*, vol. 57, no. 2, pp. 667–682, 2018.
- [36] Q. Yuan, Q. Zhang, J. Li, H. Shen, and L. Zhang, "Hyperspectral image denoising employing a spatial-spectral deep residual convolutional neural network," *IEEE Transactions on Geoscience and Remote Sensing*, vol. 57, no. 2, pp. 1205–1218, 2018.
- [37] Q. Shi, X. Tang, T. Yang, R. Liu, and L. Zhang, "Hyperspectral image denoising using a 3-d attention denoising network," *IEEE Transactions on Geoscience and Remote Sensing*, vol. 59, no. 12, pp. 10 348–10 363, 2021.
- [38] K. Wei, Y. Fu, and H. Huang, "3-d quasi-recurrent neural network for hyperspectral image denoising," *IEEE Transactions on Neural Networks and Learning Systems*, vol. 32, no. 1, pp. 363–375, 2020.
- [39] B. Lin, X. Tao, and J. Lu, "Hyperspectral image denoising via matrix factorization and deep prior regularization," *IEEE Transactions on Image Processing*, vol. 29, pp. 565–578, 2019.
- [40] X. Cao, X. Fu, C. Xu, and D. Meng, "Deep spatial-spectral global reasoning network for hyperspectral image denoising," *IEEE Transactions on Geoscience and Remote Sensing*, vol. 60, pp. 1–14, 2021.
- [41] L. Pang, W. Gu, and X. Cao, "Trq3dnet: A 3d quasi-recurrent and transformer based network for hyperspectral image denoising," *Remote Sensing*, vol. 14, no. 18, 2022.
- [42] F. Xiong, S. Tao, J. Zhou, J. Lu, J. Zhou, and Y. Qian, "Smds-net: Model guided spectral-spatial network for hyperspectral image denoising," *arXiv preprint arXiv:2012.01829*, 2020.
- [43] T. Bodrito, A. Zouaoui, J. Chanussot, and J. Mairal, "A trainable spectral-spatial sparse coding model for hyperspectral image restoration," *Advances in Neural Information Processing Systems*, vol. 34, pp. 5430–5442, 2021.
- [44] F. Xiong, J. Zhou, Q. Zhao, J. Lu, and Y. Qian, "Mac-net: Model-aided nonlocal neural network for hyperspectral image denoising," *IEEE Transactions on Geoscience and Remote Sensing*, vol. 60, pp. 1–14, 2021.
- [45] Y. Q. Dai Wenyuan, X. Guirong, and Y. Yong, "Boosting for transfer learning," in *International Conference on Machine Learning*, 2007, pp. 193–200.
- [46] M. Mahmud and S. Ray, "Transfer learning using kolmogorov complexity: Basic theory and empirical evaluations," *Advances in Neural Information Processing Systems*, vol. 20, 2007.
- [47] S. Ben-David, J. Blitzer, K. Crammer, A. Kulesza, F. Pereira, and J. W. Vaughan, "A theory of learning from different domains," *Machine Learning*, vol. 79, no. 1, pp. 151–175, 2010.
- [48] C. Cortes and M. Mohri, "Domain adaptation in regression," in *International Conference on Algorithmic Learning Theory*. Springer, 2011, pp. 308–323.
- [49] P. Germain, A. Habrard, F. Laviolette, and E. Morvant, "A new pac-bayesian perspective on domain adaptation," in *International Conference on Machine Learning*. PMLR, 2016, pp. 859–868.
- [50] D. McNamara and M.-F. Balcan, "Risk bounds for transferring representations with and without fine-tuning," in *International Conference on Machine Learning*. PMLR, 2017, pp. 2373–2381.
- [51] G. Blanchard, G. Lee, and C. Scott, "Generalizing from several related classification tasks to a new unlabeled sample," *Advances in Neural Information Processing Systems*, vol. 24, 2011.
- [52] K. Muandet, D. Balduzzi, and B. Schölkopf, "Domain generalization via invariant feature representation," in *International Conference on Machine Learning*. PMLR, 2013, pp. 10–18.
- [53] G. Blanchard, A. A. Deshmukh, Ü. Dogan, G. Lee, and C. Scott, "Domain generalization by marginal transfer learning," *The Journal of Machine Learning Research*, vol. 22, no. 1, pp. 46–100, 2021.
- [54] A. Sicilia, X. Zhao, and S. J. Hwang, "Domain adversarial neural networks for domain generalization: When it works and how to improve," *arXiv preprint arXiv:2102.03924*, 2021.
- [55] A. Maurer, M. Pontil, and B. Romera-Paredes, "The benefit of multitask representation learning," *Journal of Machine Learning Research*, vol. 17, no. 81, pp. 1–32, 2016.
- [56] N. Tripurani, M. Jordan, and C. Jin, "On the theory of transfer learning: The importance of task diversity," *Advances in Neural Information Processing Systems*, vol. 33, pp. 7852–7862, 2020.
- [57] J. Shu, D. Meng, and Z. Xu, "Learning an explicit hyperparameter prediction policy conditioned on tasks," *arXiv preprint arXiv:2107.02378*, 2021.
- [58] Z. Qiu, T. Yao, and T. Mei, "Learning spatio-temporal representation with pseudo-3d residual networks," in *Proceedings of the IEEE International Conference on Computer Vision*, 2017, pp. 5533–5541.
- [59] W. Shi, Q. Ling, G. Wu, and W. Yin, "A proximal gradient algorithm for decentralized composite optimization," *IEEE Transactions on Signal Processing*, vol. 63, no. 22, pp. 6013–6023, 2015.
- [60] Y. Sun, Y. Yang, Q. Liu, J. Chen, X.-T. Yuan, and G. Guo, "Learning non-locally regularized compressed sensing network with half-quadratic splitting," *IEEE Transactions on Multimedia*, vol. 22, no. 12, pp. 3236–3248, 2020.
- [61] S. Boyd, N. Parikh, E. Chu, B. Peleato, J. Eckstein *et al.*, "Distributed optimization and statistical learning via the alternating direction method of multipliers," *Foundations and Trends® in Machine Learning*, vol. 3, no. 1, pp. 1–122, 2011.
- [62] Z. Lin, M. Chen, and Y. Ma, "The augmented lagrange multiplier method for exact recovery of corrupted low-rank matrices," *arXiv preprint arXiv:1009.5055*, 2010.
- [63] H. Zhang, L. Liu, W. He, and L. Zhang, "Hyperspectral image denoising with total variation regularization and nonlocal low-rank tensor decomposition," *IEEE Transactions on Geoscience and Remote Sensing*, vol. 58, no. 5, pp. 3071–3084, 2019.
- [64] B. Rasti, M. O. Ulfarsson, and P. Ghamisi, "Automatic hyperspectral image restoration using sparse and low-rank modeling," *IEEE Geoscience and Remote Sensing Letters*, vol. 14, no. 12, pp. 2335–2339, 2017.
- [65] J. Peng, Y. Wang, H. Zhang, J. Wang, and D. Meng, "Exact decomposition of joint low rankness and local smoothness plus sparse matrices," *IEEE Transactions on Pattern Analysis and Machine Intelligence*, pp. 1–16, 2022.
- [66] D. Ulyanov, A. Vedaldi, and V. Lempitsky, "Deep image prior," in *Proceedings of the IEEE Conference on Computer Vision and Pattern Recognition*, 2018, pp. 9446–9454.
- [67] J. Lehtinen, J. Munkberg, J. Hasselgren, S. Laine, T. Karras, M. Aittala, and T. Aila, "Noise2noise: Learning image restoration without clean data," in *International Conference on Machine Learning*. PMLR, 2018, pp. 2965–2974.
- [68] Y.-S. Luo, X.-L. Zhao, T.-X. Jiang, Y.-B. Zheng, and Y. Chang, "Hyperspectral mixed noise removal via spatial-spectral constrained unsupervised deep image prior," *IEEE Journal of Selected Topics in Applied Earth Observations and Remote Sensing*, vol. 14, pp. 9435–9449, 2021.
- [69] M. Mohri, A. Rostamizadeh, and A. Talwalkar, *Foundations of machine learning*. MIT press, 2018.
- [70] P. L. Bartlett and S. Mendelson, "Rademacher and gaussian complexities: Risk bounds and structural results," *Journal of Machine Learning Research*, vol. 3, no. Nov, pp. 463–482, 2002.
- [71] N. Parikh, S. Boyd *et al.*, "Proximal algorithms," *Foundations and Trends® in Optimization*, vol. 1, no. 3, pp. 127–239, 2014.
- [72] X. Xie, Q. Wang, Z. Ling, X. Li, G. Liu, and Z. Lin, "Optimization induced equilibrium networks: An explicit optimization perspective for understanding equilibrium models," *IEEE Transactions on Pattern Analysis and Machine Intelligence*, pp. 1–14, 2022.